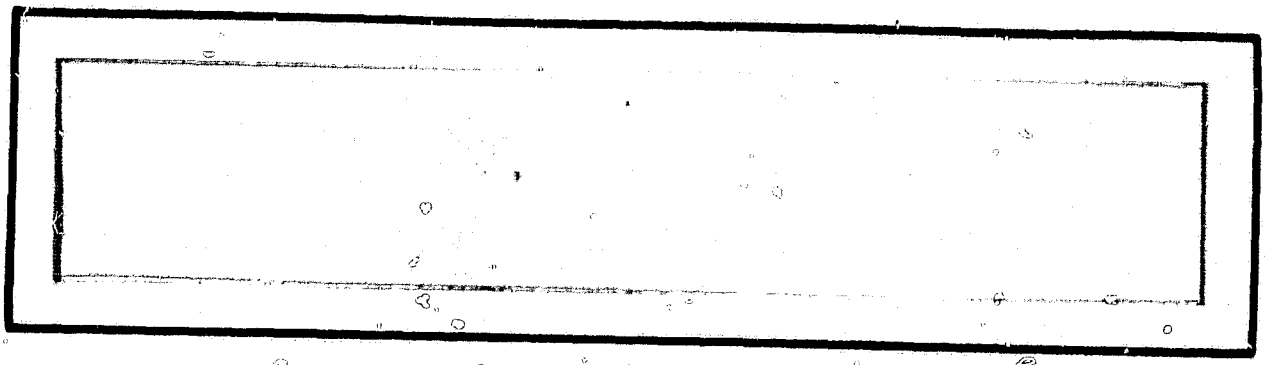

Axiomatix

# RANGING/TRACKING SYSTEM FOR PROXIMITY OPERATIONS

FINAL REPORT

Contract No. NAS9-15666

Prepared for

NASA Lyndon B. Johnson Space Center
Houston, Texas 77058

Prepared by

Peter Nilsen

Axiomatix
9841 Airport Blvd., Suite 912
Los Angeles, California 90045

Axiomatix Report No. R8206-1
June 3, 1982

TABLE OF CONTENTS

## LIST OF FIGURES

# 1.0 INTRODUCTION

This report documents the hardware development and testing phase of a hand-held radar for the ranging and tracking for Shuttle proximity operations. The radar is shown in Figure 1.1. A trade-off study and system design of the radar was performed under Phase I of Contract No. NAS 9-15666, as documented in Axiomatix Report No. R7901-5, dated January 30, 1979. A picture of the completed radar is given in Figure 1.1.

The detailed circuit design and fabrication of the radar was performed by Kustom Electronics under subcontract to Axiomatix. This arrangement provided the maximum radar capability at the lowest possible cost due to Kustom's background and experience with velocity-only police radars. Throughout the hardware development, Axiomatix worked closely with Kustom, especially in the areas of hardware decisions which affected the overall radar performance. The effectiveness of this arrangement is substantiated by the close degree to which the radar meets the original performance goals.

To put things into perspective, it is helpful to briefly compare the radar's performance goals with some of the field test results. The radar is to measure range to a $3\sigma$-accuracy of 1 m (3.28 ft) to a maximum range of 1850 m (6000 ft). It is also to measure velocity to a $3\sigma$-accuracy of 0.03 m/s (0.1 ft/s). Furthermore, the radar was to be of a size and weight similar to hand-held radars frequently seen in use by motorcycle police officers. It must be stressed that these goals were to be met for a target in free space, i.e., no clutter or multiple target returns. This latter condition was very difficult to obtain in the testing program; however, as a general indication of the radar's performance, at a range of approximately 700 m, the $3\sigma$-range error was found to be 0.96 m. It is felt that much of this error is due to clutter in the test environment. As an example of the velocity accuracy, at a range of 450 m, a $3\sigma$-velocity error of 0.02 m/s was measured.

In Section 2 of this report, the principles of the radar are given. Also, a description of the radar design is given as well as design changes made since the CDR. A description of the field tests of the radar as well as the actual performance obtained is given in Section 3. Finally, in Section 4, recommended changes to the radar design are given.

Appendix B contains some of the analyses performed by Axiomatix in support of the design process, Appendix B contains the actual circuit diagrams, and the software listing is given in Appendix C.

## 2.0 RADAR DESCRIPTION

This section provides a general description of the proximity radar. The radar is an FM-CW solid-state K-band (24 GHz) radar which utilizes its microprocessor computer to extract highly accurate range and velocity measurements. It is of the same general size, shape and weight (4 lbs) of a police hand-held radar and it operates from the same type of 12-volt battery pack. Table 2.1 gives a summary of the radar's overall physical characteristics. Based on limited testing, it is believed that the radar meets or nearly meets most of these goals. The degree to which these goals are met will be established by means of comprehensive testing performed by NASA Johnson Space Center (JSC) utilizing the superior JSC technical facilities. The following section given the details of the radar's principles of operation.

Table 2.1. Summary of Proximity Radar's Characteristics

| | |
|---|---|
| Size | Approx. 10x12x3.5" (same approx. size as the hand-held police speed radar) |
| Weight | 4 lbs |
| Power requirements | 12 V (normally supplied by battery pack) |
| Frequency of operation | 24 GHz (nominal) |
| Antenna beamwidth | 9° (3 dB) |
| Antenna Gain | 26 dB |
| Maximum design range | 6000 ft |
| Design goal range accuracy | $\sigma$ = 0.33 m |
| Design goal velocity accuracy | $\sigma$ = 0.1 m/s |

## 2.1 Principles of Operation

A top-level functional block diagram of the radar system is given in Figure 2.1. The tunable K-band transmitter is based on a variable-Gunn oscillator whose frequency is ramped up and down according to a sawtooth pattern. The received signal also ramps up and down but, because of range delay, the frequency of the received signal at any instant of time differs from the transmitted signal. This difference or beat note is proportional to the range and is extracted by means of the receiver mixer. This process, and the radar functional block diagram, is explained in greater detail in the following paragraphs.

Figure 2.2 shows a functional block diagram of the proposed radar sensor system. The system is an FM-CW solid-state K-band (24 GHz) radar which extracts both the range and velocity information from the baseband signals i.e., 0 IF) receiver. Generation of all the timing signals, as well as processing of the raw received data, is performed by a Motorola MC68701 microprocessor which forms the System Controller and Data-Processing (SCDP) unit.

The transmitter portion of the radar sensor system is comprised of a modulation waveform generator, two Gunn K-band oscillators, a microwave mixer, and a counter. The modulation waveform generator provides the waveform needed for varying the frequency of the radar transmitter and contains a modulation-linearizer circuit. The waveform is a triangular function whose frequency is selected according to the mode of the radar operation. This waveform is applied to the frequency control terminal of a K-band voltage-controlled oscillator (VCO), thus resulting in a frequency modulation of the oscillators' output.

The frequency-modulated K-band carrier is then applied via a turnstile diplexer to the radar antenna. The nominal (unmodulated) RF frequency of the K-band transmitter is 24 GHz and the nominal output power is 200 mW.

In order to provide for accurate control of the transmitter frequency deviation $\Delta F$ (nominal $\Delta F = 100$ MHz), the RF output of the transmitter VCO is sampled and mixed with an RF signal developed by a stable, high-Q, Gunn-type phase-locked local oscillator (LO). The frequency of the LO is such that the lower difference frequency between it and the frequency-modulated VCO varies between 500 and 600 MHz, approximately. The difference frequency is applied to a 16-bit counter which determines the lower and upper extremes of the frequency excursion of the transmitted signal. The frequency counts corresponding to the

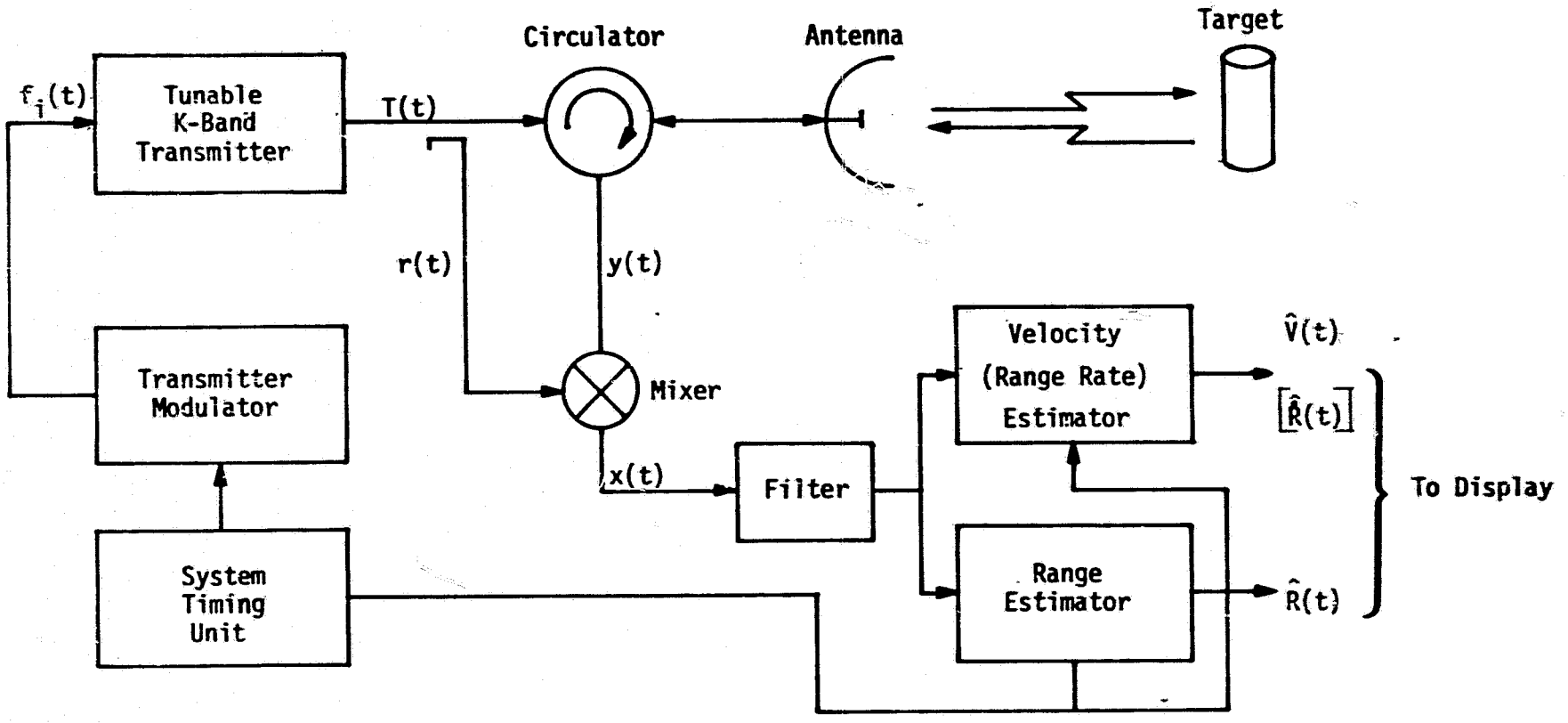


Figure 2.1.- Functional Block Diagram of Radar Ranging and Tracking System

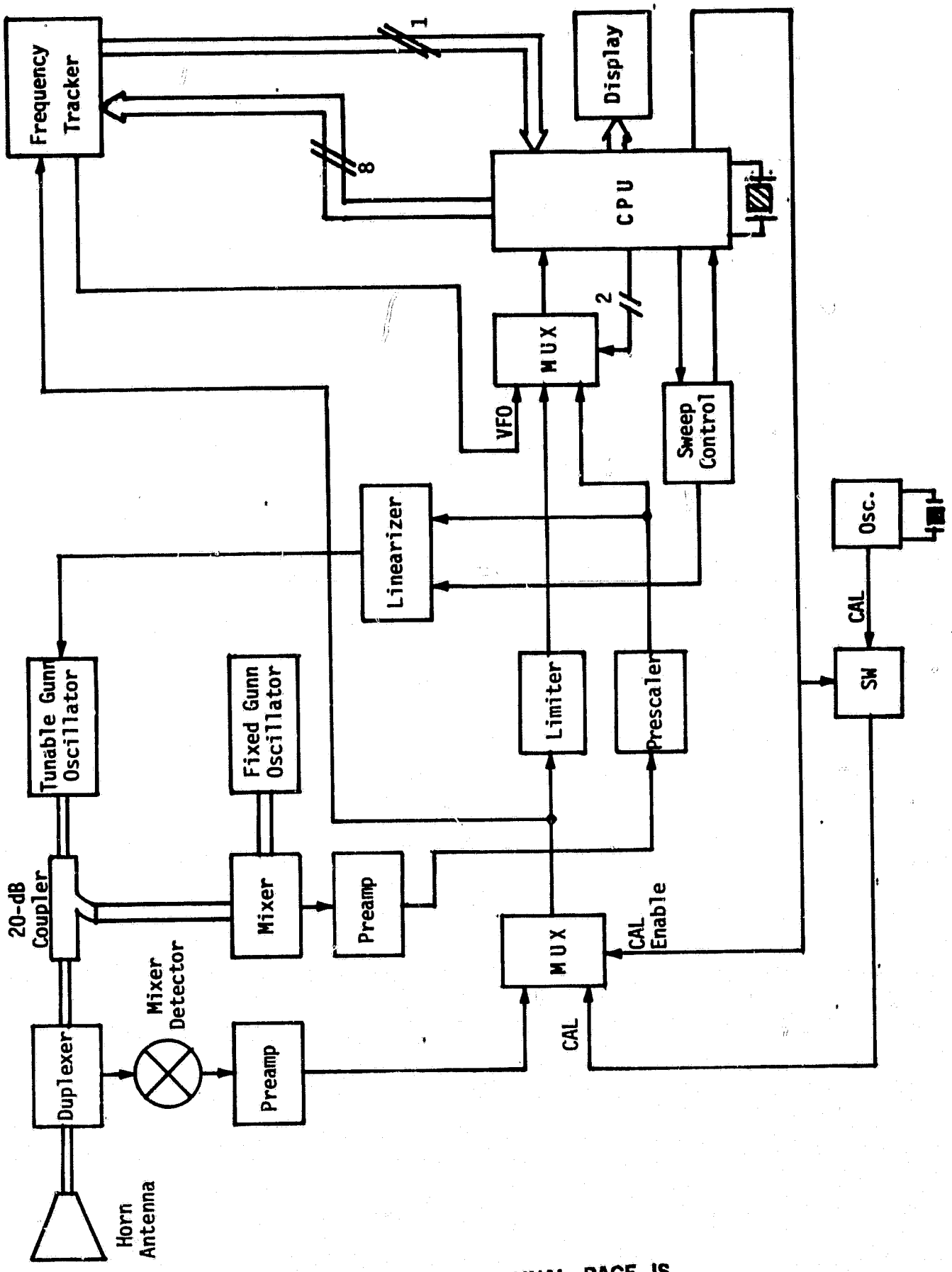


Figure 2.2. Radar Detailed Functional Block Diagram

lower and upper extremes are performed upon the "frequency high" and "frequency low" commands developed by the modulation waveform generator. These commands are delivered to the system controller which, in turn, commands the modulator to continue the frequency sweep in the opposite direction.

The exact time duration measurement of both the frequency-up and frequency-down swings is provided by counting the number of pulses developed by a time-base generator during the frequency sweep interval. This number is measured by time-sharing a single 16-bit counter between the RF frequency and the time-reference pulse counts. The purpose of the precise time interval measurement is to obtain tn accurate value of $\Delta t_m$ which, combined with an accurately measured value of $\Delta F$, can provide the data processor with all the information required to calculate the frequency sweep slope S in MHz/s, the latter being defined as $\Delta F/\Delta t_m$. Because the slope plays an important role in determining the accuracy of the proposed system, such "dynamic" determination of the slope eliminates the major bias inaccuracies associated with component value changes in the FM-CW transmitter circuitry.

The receiver of the proposed radar sensor system is a homodyne receiver, also known as a "0 IF" receiver. As shown in the block diagram of Figure 2.2, the receiver consists of a mixer followed by a preamplifier. The preamplifier also includes the required filtering an an Automatic Gain Control (AGC) function.

As shown in Figure 2.2, the receiver mixer has only one RF input. This is because the second signal, i.e., the LO, is an attenuated fraction of the transmitted signal itself. The controlled degree of the transmitted signal attenuation is provided by the turnstile diplexer unit. This unit delivers the VCO output to the antenna and couples only a small fraction of the transmitted signal to the receiver mixer; there this LO is mixed with the signal received from the target, thus resulting in the baseband tones which are applied to the receiver amplifier and filter.

The receiver has three measurement modes corresponding to short, medium and long ranges. The ranges for these modes are defined in Table 2.2. In the short-range mode, ths frequency of the received baseband range tone (or tones, for the case of a moving target) is determined by direct frequency counting by the microprocessor frequency counter. However, in the medium- and long-range modes, the tone(s) are first tracked by the frequency tracker so as to improve the tone signal-to-noise ratio prior to frequency measurement. In

Table 2.2. Radar Modes

| Mode | Range Start | Range Stop | Time to Search | Tracker $B_L$ |
|---|---|---|---|---|
| Short-Range | 2.7 m | 120 M | 0 - 2 s | - |
| Medium-Range | 40 m | 600 M | 0 - 7 s | 200 Hz |
| Long-Range | 300 m | 2500 M | 0 - 16 s | 50 Hz |

actuality, one frequency tracker is time multiplexed between the two tones for the case of a moving target.

Figure 2.3 shows the frequency/time pattern which the radar uses. Part (a) shows the relationship between the transmitter and the received signals. Because of the homodyne configuration of the proposed system, the transmitted and LO signals are the same (except for the power level); therefore, the time/frequency relationships shown in part (a) also applies to the LO signal/received signal pattern.

As a result of the mixer action, a beat note appears at the baseband output of the mixer. For the case of a stationary target such as that illustrated in Figure 2.3, the frequency of this beat note is proportional to the slope of the transmitter frequency modulation waveform and the round-trip time to the target. Expressed quantitatively, this relationship is

$$f_r = \frac{\Delta F}{\frac{1}{2f_m}} \left(\frac{2R}{c}\right) = \frac{4Rf_m\Delta F}{c} \qquad (1a)$$

$$= ST_d \qquad (1b)$$

where

$f_r$ = frequency of the baseband beat note proportional to the target range, henceforth referred to as "range frequency" or "range tone"

$f_m$ = modulation waveform repetition frequency

$R$ = target range in meters (m)

$c$ = $3\times10^8$ meters/second (m/s)

$T_d$ = target round-trip delay time

$\Delta F$ = peak-to-peak frequency deviation, Hz

$S$ = linear FM modulation slope, Hz/s

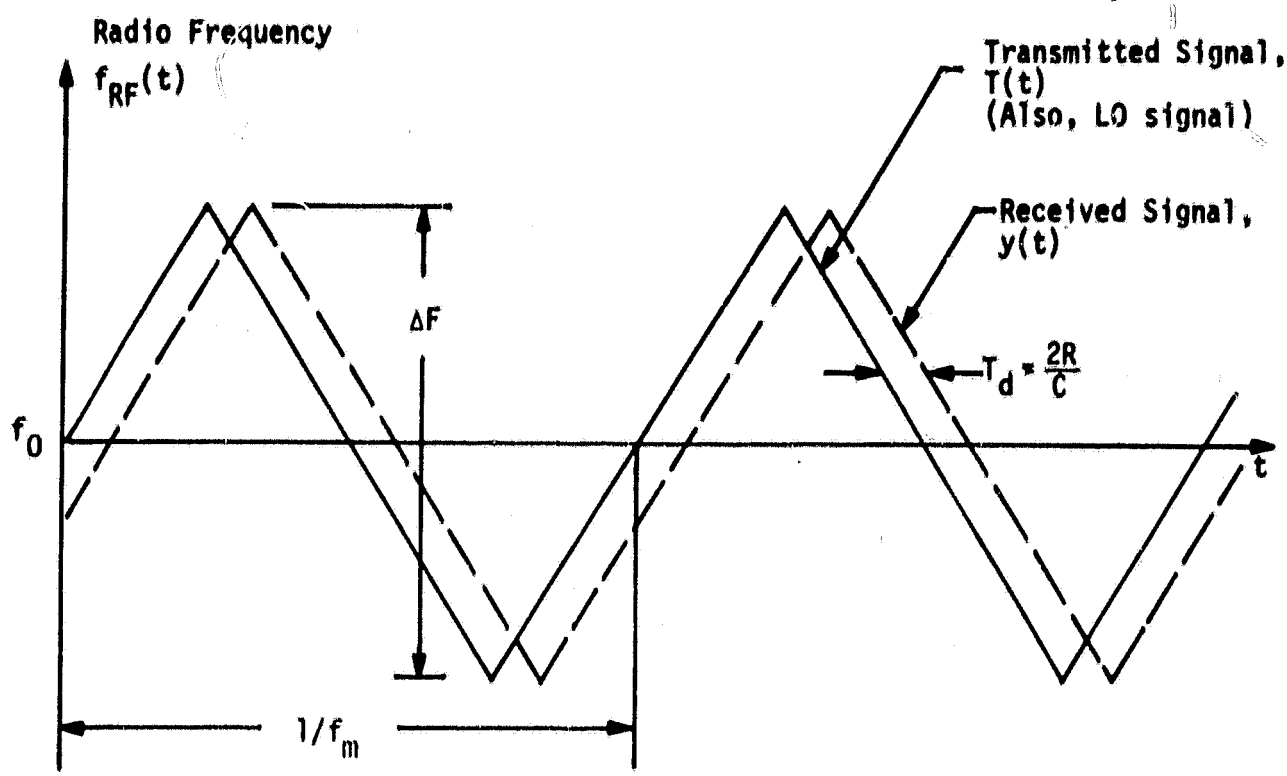


= 0.105 s Short- and Medium-Range Mode
= 0.355 s Long-Range Mode

(a) Transmitted and Received RF Signals

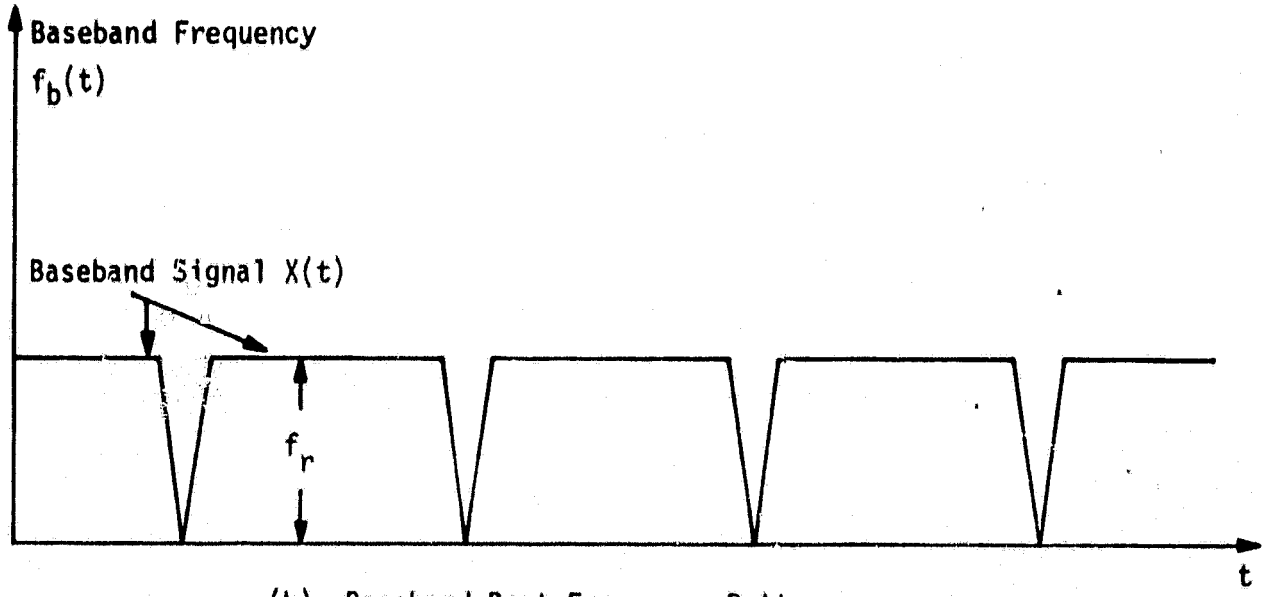


(b) Baseband Beat Frequency Pattern

Figure 2.3. Frequency/Time Pattern of the Proximity Radar for a Stationary Target

When the target is moving and its motion has a radial component along the direction towards the radar, the reflected signal will be shifted in frequency by the amount quantitatively defined by the following expression:

$$f_d = \frac{2V}{\lambda} + \frac{2Vf_0}{c} \tag{2}$$

where $f_d$ is the apparent shift in target velocity, V is the target velocity in m/s (along a radial to the radar), and $f_0$ is the transmitter frequency. The frequency shift $f_d$ is commonly referred to as the "doppler shift" and, depending on the direction of the velocity, this shift can cause either an apparent increase or a decrease in the received signal.

When the target is approaching the radar, the frequency of the received signal is higher than the transmitted frequency. Therefore, the output of the mixer, which is the difference frequency between the transmitted and received signals, contains a component proportional to the doppler shift. Thus, for an approaching target and during the positive-slope portion of the angle, the output of the mixer is

$$f_L = \left| St - \left[ S(t - T_d) + \frac{2Vf_0}{c} \right] \right| = ST_d - \frac{2Vf_0}{c} \text{ for V and S positive}$$
$$= f_r - f_d \tag{3}$$

The absolute brackets are used to indicate that, with a zero IF receiver, all the RF shifts appear only as positive frequencies at the baseband.

During the negative-slope portion of the cycle, the beat note frequency for an approaching target is

$$f_U = \left| -St - \left[ -S(t - T_d) + \frac{2Vf_0}{c} \right] \right| = \left| -sT_d - \frac{2Vf_0}{c} \right| \text{ for V positive and S negative}$$
$$= sT_d + \frac{2Vf_0}{c} = f_r + f_d \tag{4}$$

The situation defined by (3) and (4) is shown in Figure 2.4. Part (b) of this figure is particularly indicative of this time/frequency relationship at baseband, as shown there, the frequencies $f_U$ and $f_L$ refer to the upper and lower frequencies observed for a particular target situation.

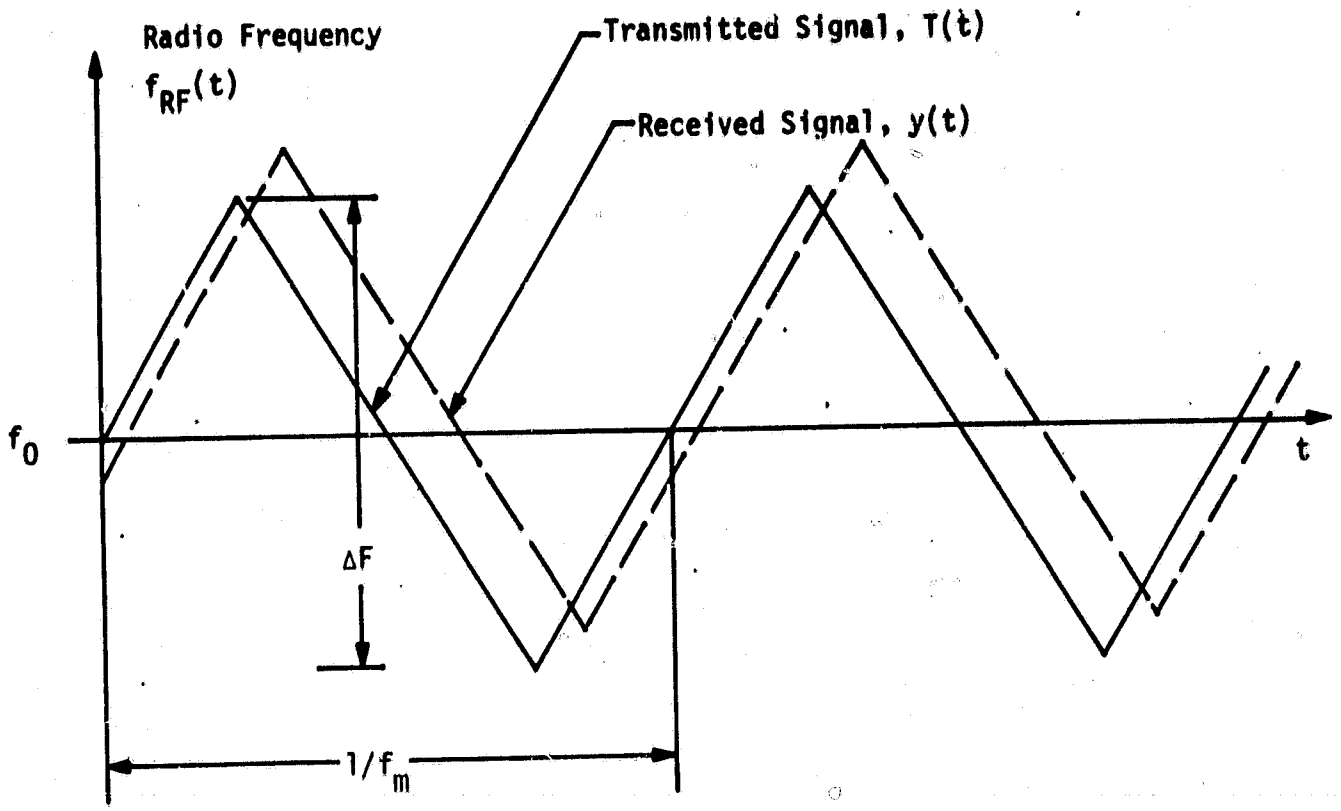


(a) Transmitted and Received RF Signals

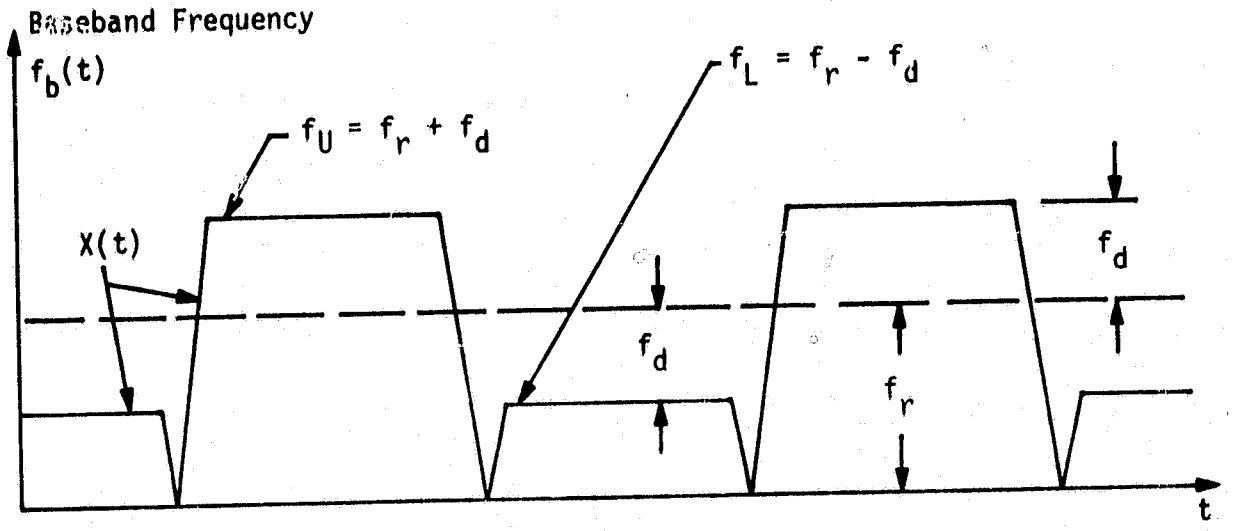


(b) Baseband Beat Frequency Pattern

Figure 2.4. Frequency/Time Pattern of the Proximity Radar When the Received Signal Return Frequency Includes Doppler Shift (Target Approaching)

For a receding target, the frequency/time relationship at baseband is the reverse of that for an approaching target. Specifically, the higher beat note will be developed during the positive-slope portion of the cycle, and the lower beat note will appear at the output of the mixer during the negative slope. This "role reversal" relationship between $f_U$, $f_L$ and the positive and negative slopes of the modulation cycle provides the information required to determine the direction of the target motion.

The range and doppler frequencies are extracted from $f_U$ and $f_L$ in the following manner:

$$f_r = \frac{f_U + f_L}{2} \tag{5a}$$

and

$$f_d = \frac{f_U - f_L}{2} \tag{5b}$$

The above evaluations form the basis of the computations performed by the radar's microprocessor computer to extract range and velocity. The actual equations for range and velocity solved by the microprocessor computer are

$$R = (f_U + f_L)\frac{c}{2\Delta f}\left(\frac{\Delta T_a\,\Delta T_b}{\Delta T_a + \Delta T_b}\right)$$

$$V = \frac{c}{4f_0}\left[f_U - f_L + (f_U - f_L)\frac{\Delta T_a - \Delta T_b}{\Delta T_a + \Delta T_b}\right]$$

where $\Delta T_a$ is the time interval during the sweep up and $\Delta T_b$ is the time interval during the sweep down (both measured by the microprocessor).

## 2.2 Design Changes Since the CDR

The radar design is essentially the same as that which existed at the CDR, with one main exception: the addition of a linearizer circuit to the modulation waveform control. The purpose of this circuit is to make the frequency variation of the varactor-tuned transmitter Gunn oscillator a very linear function of tuning voltage. This is necessary in order to eliminate frequency chirp on the baseband tones which would prevent the frequency tracker from acquiring in medium- and long-range modes. The chirp does not affect the radar accuracy,

however, as shown analytically by Axiomatix and verified during the breadboard test made at the CDR. The linearizer approach was suggested by Sergei Udalov of Axiomatix and successfully implemented by John Aker. A functional block diagram of the linearizer is given in Figure 2.5.

This linearizer system effectively phase locks the tuned Gunn to the voltage-to-frequency converter (VFC) which is highly linear; however, the penalty paid is that any phase jitter on the VFC appears on the Gunn oscillator output but multiplied by the divider ratio. Axiomatix's analysis, given in Appendix A, verified this problem and led to the selection of a low-noise VFC.

Another hardware change made since the CDR was the substitution of a different fixed-Gunn oscillator. The original Gunn was relatively stable with temperature, while the tuned-Gunn drifted with temperature. Thus, while testing on the frozen wasteland of the Kansas winter prairie, it was found that the offset between the two oscillators changed so much in cold weather that the difference frequency was outside the lock range of the linearizer. This was remedied by substituting a Gunn oscillator that more closely tracked the tunable Gunn as a function of temperature.

## 2.3 Hardware Description

The radar hardware consists of five printed-circuit boards, a liquid crystal display and a microwave assembly that includes the horn antenna. These subassemblies are mounted in an aluminum case which is a modified Kustom HR4 police radar case. A top-view drawing of these subassemblies is shown in Figure 2.6, and an exploded-view drawing is given in Figure 2.7. These drawings indicate the mounting relationship among all the subassemblies. The mother board serves to electrically connect all the boards. The schematics for each PCB as well as the interconnect diagram and PCM assembly drawings are given in Appendix B.

## 2.4 Software Description

The radar microprocessor software performs the entire control of the radar, including calibration, mode selection, hardware control and data processing. This software consists of approximately 1000 lines of machine code and completely fills the 2-kbyte ROM on the MC68701 processor chip. A software flowchart was presented at the CDR; however, since the software was revised, this flowchart is no longer applicable. In lieu of an updated flowchart, a complete listing of the software which is carefully commented on is given in Appendix C.

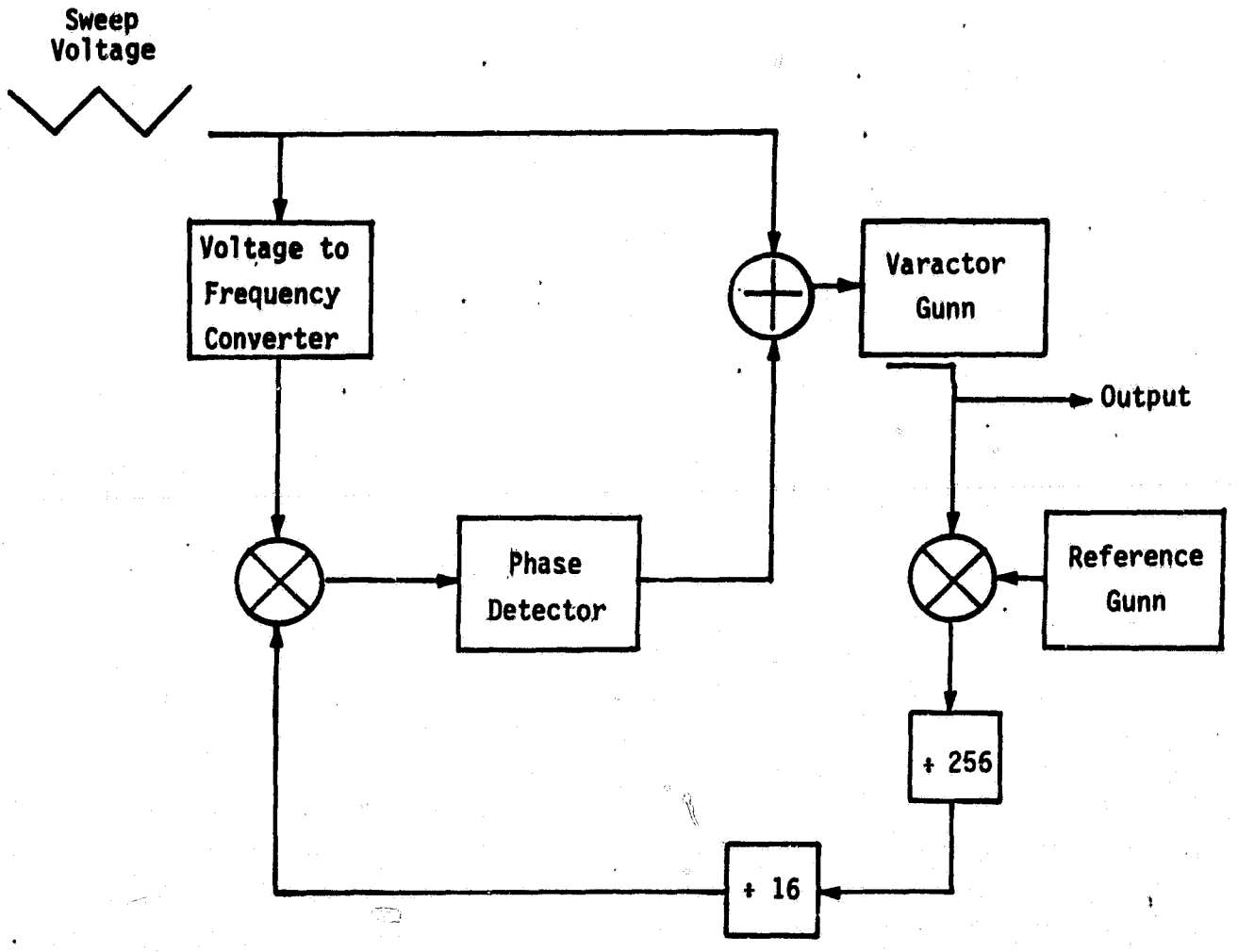


Figure 2.5. Block Diagram of Modulation Linearizer

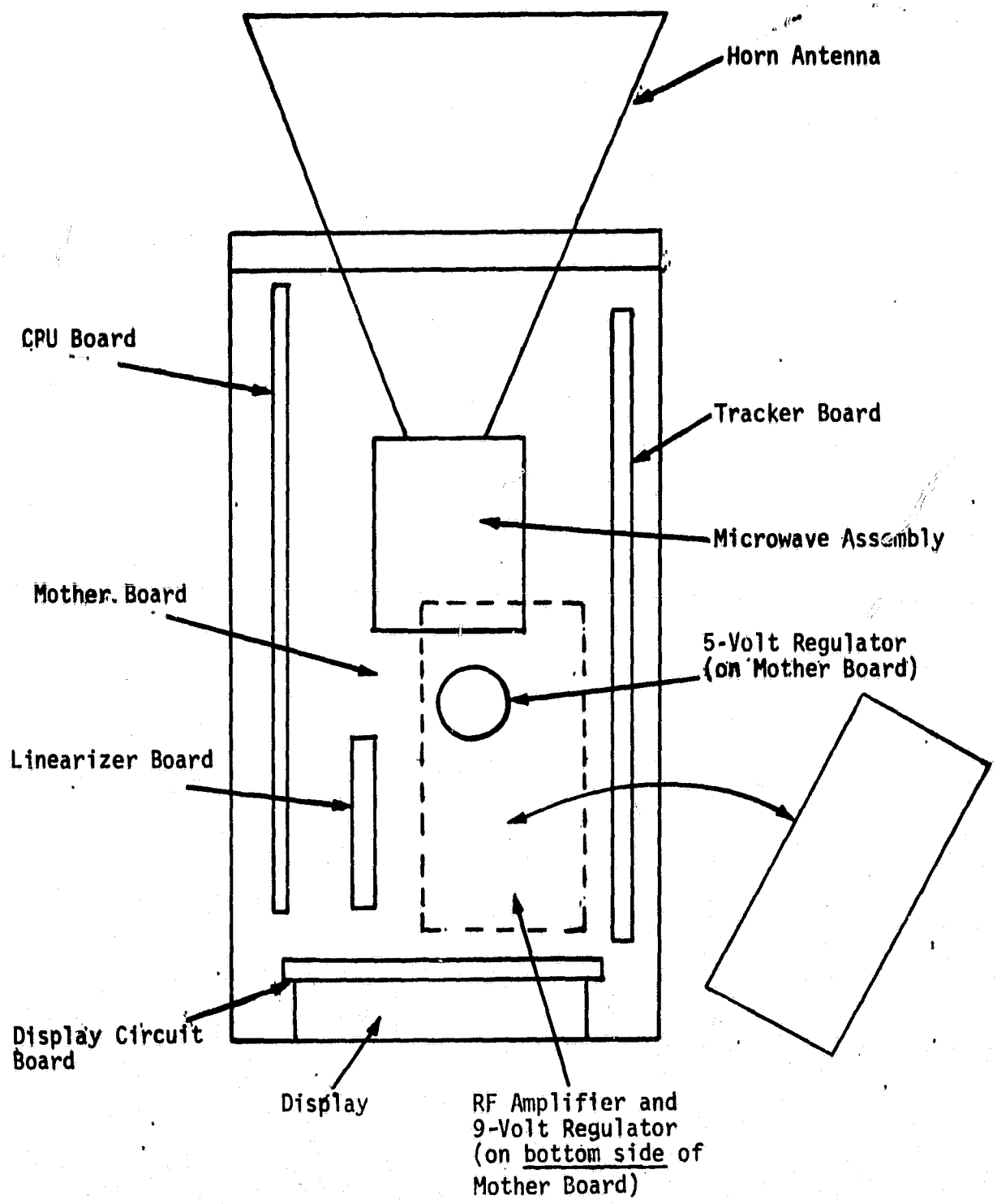


Figure 2.6. Radar Top View

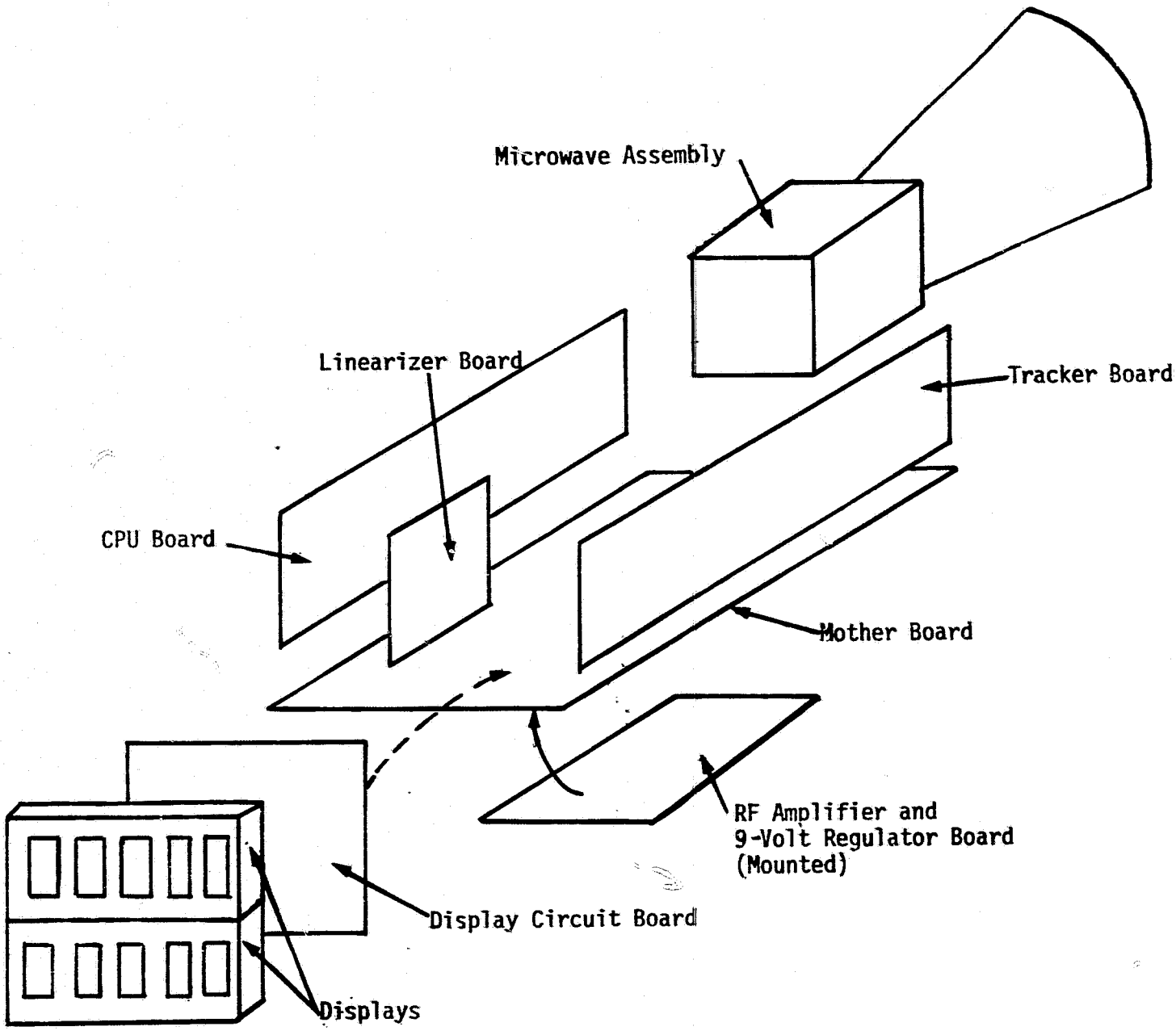


Figure 2.7. Radar Exploded View

# 3.0 RADAR TEST

This section describes the field tests performed by Axiomatix and Kustom, with NASA present, to verify the radar performance. Also presented in this section is the test data and comparisons of measured radar performance with performance goals.

## 3.1 Test Description

Field tests were conducted to determine how well the radar design meets the performance goals. The scope and credibility of the tests were limited by the problem of obtaining a simple radar target in free space, i.e., no clutter or backscatter, at long ranges within the cost limitation of a low-cost development program. Furthermore, the overall development plan for the radar called for the detailed radar testing to be done as another phase, probably at NASA facilities. However, the field tests were conducted using a water tower that is 110 feet high and 22 feet in diameter (if we assume a 50% aperture efficiency, the water tower is approximately a 20-$m^2$ target). For many ranges up to a maximum of 700 m, this target was relatively clutter free. For some ranges, however, particularly those closer than the maximum, it was obvious that clutter presented a serious interference problem. This is reflected in the large variance in the range measurement values at those ranges.

Figure 3.1 shows the basic test setup for range measurements and Figure 3.2 shows two Axiomatix engineers conducting a range test. The water tower target is shown in Figure 3.3, which shows the radar being aimed at the tower. The test setup for low-speed velocity measurements is shown in Figure 3.4. This setup utilized a variable-speed winch to pull the radar mounted on a movable platform along a calibrated track. A stop watch was used to determine the exact speed and the water tower was the target. Figure 3.5 shows a low-speed velocity test in progress.

In addition to the low-speed tests, Kustom conducted several medium-speed tests from an automobile using a corner reflector as a target and a modified HR4 police radar as a calibration device, as documented in Appendix E.

## 3.2 Performance

The reduced range data is given in Figure 3.6. This figure presents the standard deviation of 1$\sigma$-range error as a function of range. The scatter of the data points is thought to be caused by multiple-target reflections and



Figure 1.1. Hand-Held Space Radar


Figure 3.1. Range Measurement Test Setup

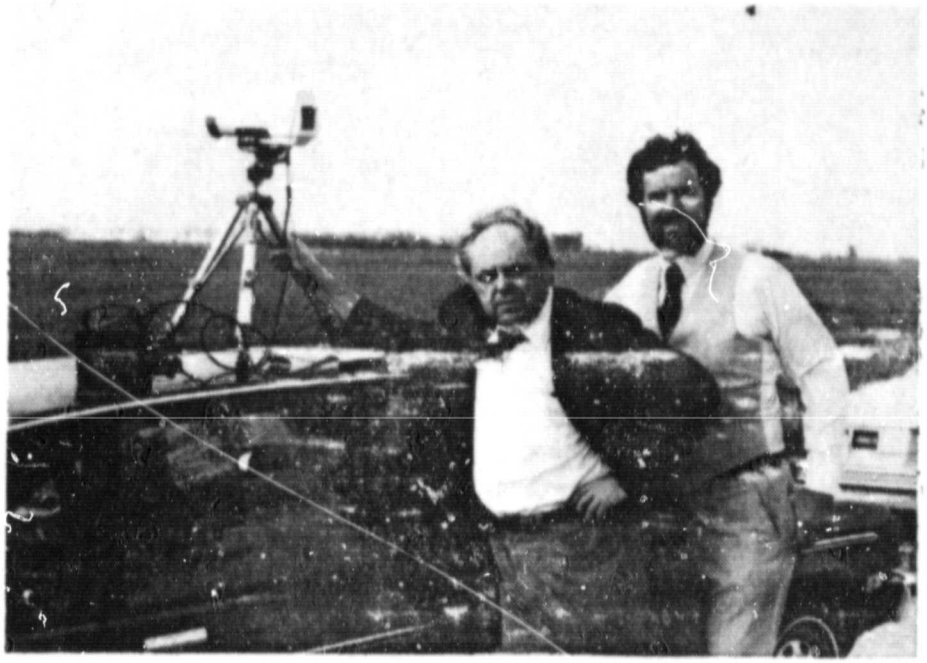

Figure 3.2. Axiomatix Engineers Conducting a Range Test

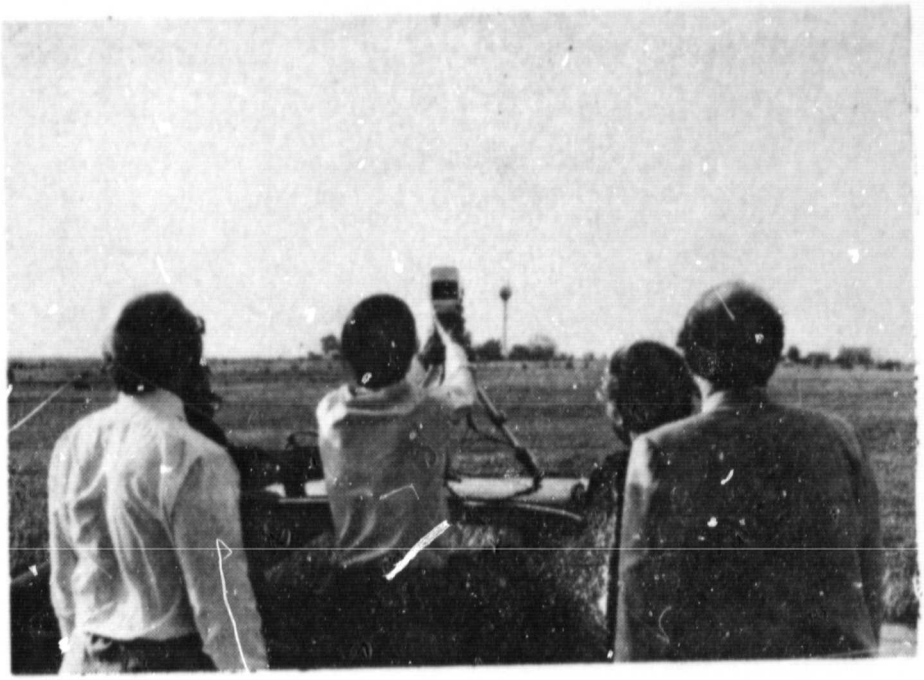

Figure 3.3. Radar Being Aimed at Water Tower (Target) at Approximately 500 Meters

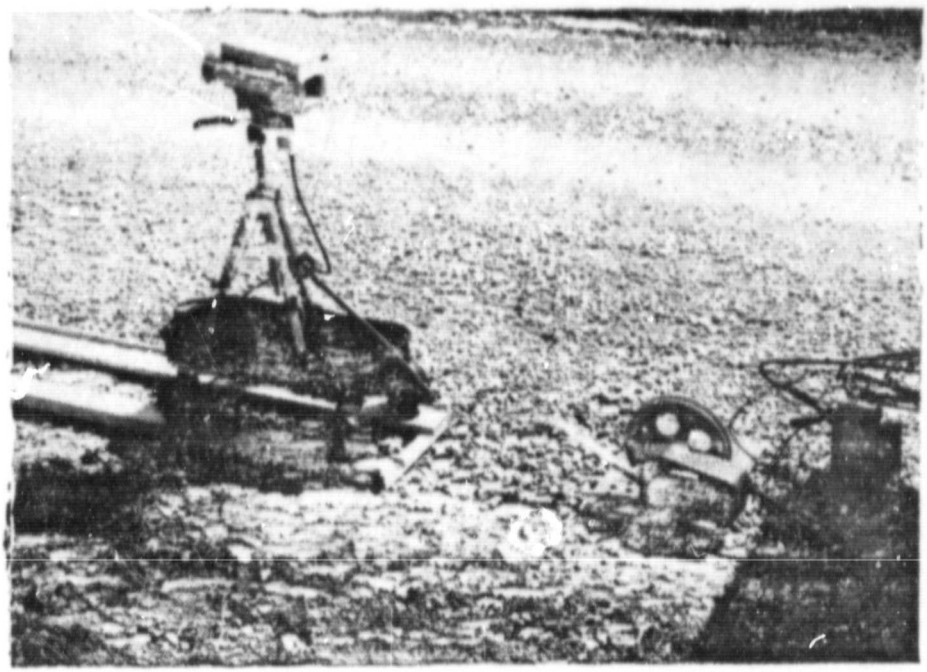

Figure 3.4. Low-Speed Velocity Test Setup

Figure 3.5. Low-Speed Velocity Test In Progress

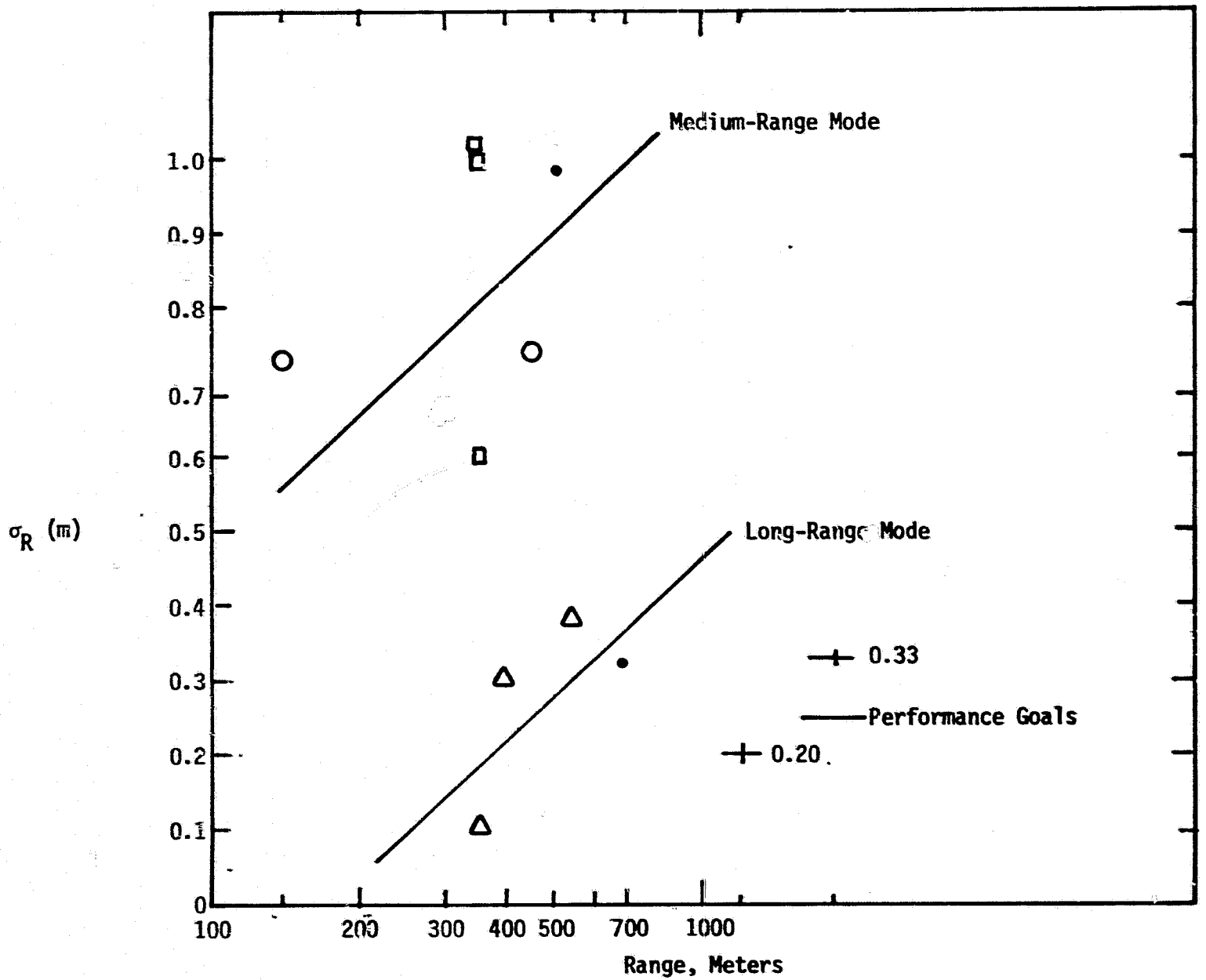


Figure 3.6 Radar Range Error versus Range

clutter. It is also felt that internal jitter in the modulation slope measurement processing may be contributing some scatter. This jitter can be remedied, and is discussed in Section 4.

Two range-error trends exist because the radar could be in either medium-range mode or long-range mode since these modes overlap in the 300 to 600 m range. The ratio of tracker bandwidths in the two modes is 200 Hz/50 Hz or 4, which means that the expected ratio of 1$\sigma$-errors should be $\sqrt{4} = 2$, which is almost exactly the ratio between the two trend lines. Comparisons between the long-range mode line and the performance goal line show that the actual 1$\sigma$-error is approximately twice the performance goal. This is considered to be an excellent agreement considering the test environment.

The 1$\sigma$-velocity error data is shown in Figure 3.7. Since relatively few measurements were made due to the difficulty in setting up the test apparatus, no trend is indicated. Again, it is felt that the scatter in data points is due to the reasons discussed for the range data scatter.

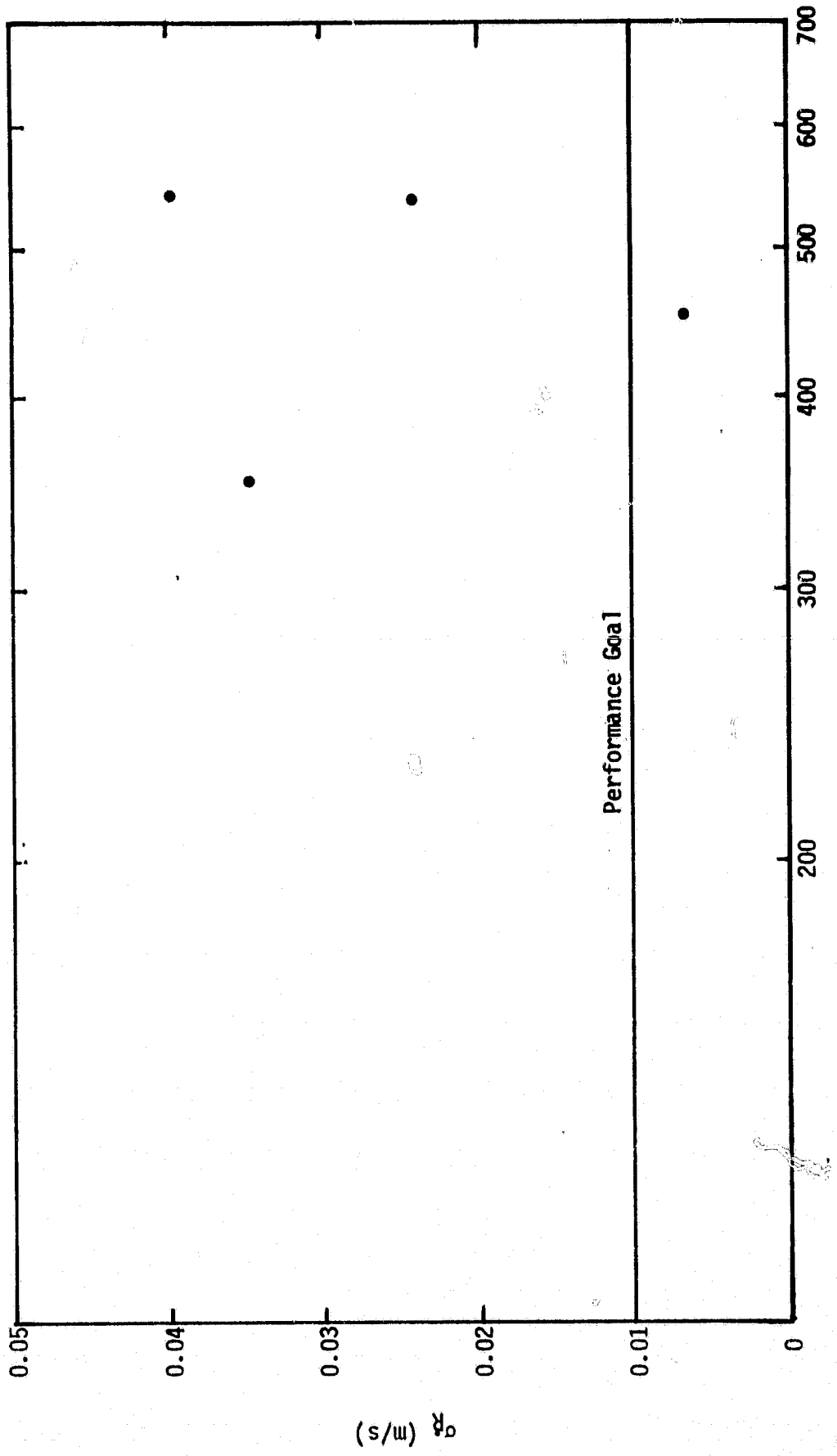


Figure 3.7. Velocity Error Data

## 4.0 RECOMMENDED CHANGES TO RADAR DESIGN

The following hardware and software modifications are recommended in order to improve the radar's performance:

(1) Redesign of power supply to provide greater voltage margin

(2) Use of a more broadband mixer diode assembly

(3) Addition of an analog signal strength meter to aid in aiming

(4) Average the ramp slope measurements to provide steadier readings

(5) Loosen up the short-range signal quality criteria

(6) Redesign the data-smoothing algorithm.

The final item, redesign of the data-smoothing algorithm, is an area where Axiomatix feels that greatly enhanced performance can be obtained at very little additional recurring cost. The need for this improvement is obvious from the scatter in the raw data. The present smoothing algorithm is a simple averager which does not take advantage of all the available information. It is suggested that a Kalman filter could vastly improve the performance. Changing the 68701 CPU to the updated Motorola version would provide an additional 2K of EPROM for such purposes as better smoothing.

## 5.0 PRECAUTIONS

Geometry and targets that can reflect more than 100 mW back into the radar should be avoided since this may burn out the mixer diodes. Also, this radar has not been mechanically designed to withstand any great amount of physical abuse. Thus, it should be treated as carefully as any other complex electronic equipment.

# APPENDIX A

## EFFECT OF VCO PHASE NOISE ON HAND-HELD RADAR

# APPENDIX A

## EFFECT OF VCO PHASE NOISE ON HAND-HELD RADAR

The following analysis was performed as part of Axiomatix's support of the circuit design effort. This analysis was performed in order to evaluate the contributions of the linearizer circuit to the radar system phase noise.

Axiomatix

9841 Airport Boulevard • Suite 912 • Los Angeles, California 90045 • Phone (213) 641-8600

TECHNICAL MEMORANDUM NO. M8204-1 DATE: April 19, 1982

TO: P. Nilsen COPIES: NAS9-15666 file

FROM: J. K. Holmes

SUBJECT: Effect of VCO Phase Noise on Hand-Held Radar

---

## 1.0 SUMMARY

Phase noise functional contributions of the Kustom Electronics hand-held radar gun are obtained for the voltage-to-frequency converter, the varactor Gunn oscillator and the reference Gunn oscillator. Based on the old voltage-to-frequency converter phase noise level, it appears that phase lock of the linearizing loop is very poor.

In addition to the closed-loop response of the linearizing loop, the delay effect on the phase noise single-sideband spectral density is considered.

It was not possible to state definitively whether or not the improved oscillator (voltage-to-frequency converter) would operate successfully since the existing theory on cycle slipping does not meaningfully apply to phase noise. It also appears that the loop bandwidth and the three-pole Butterworth filter are too close in bandwidth.

## 2.0 INTRODUCTION

The purpose of this memorandum is to document the findings obtained regarding phase noise for the hand-hald radar gun.

A varactor Gunn oscillator is driven by a sawtooth sweep voltage and, in addition, is locked to a very linear voltage-to-frequency converter which is also controlled by the sawtooth sweep voltage. The system is illustrated in Figure 1. The single-sided phase noise spectral density for the linear VCO is sketched in Figure 2.

From Figure 2, we deduce that the phase noise spectral density is given by

$$\begin{aligned} \mathcal{S}_\theta(f) &= 10^{-3.8}\left(\frac{40}{f}\right)^3 && 0 \leq f \leq 100 \\ \mathcal{S}_\theta(f) &= 10^{-5} && f \geq 100 \end{aligned} \qquad (1)$$

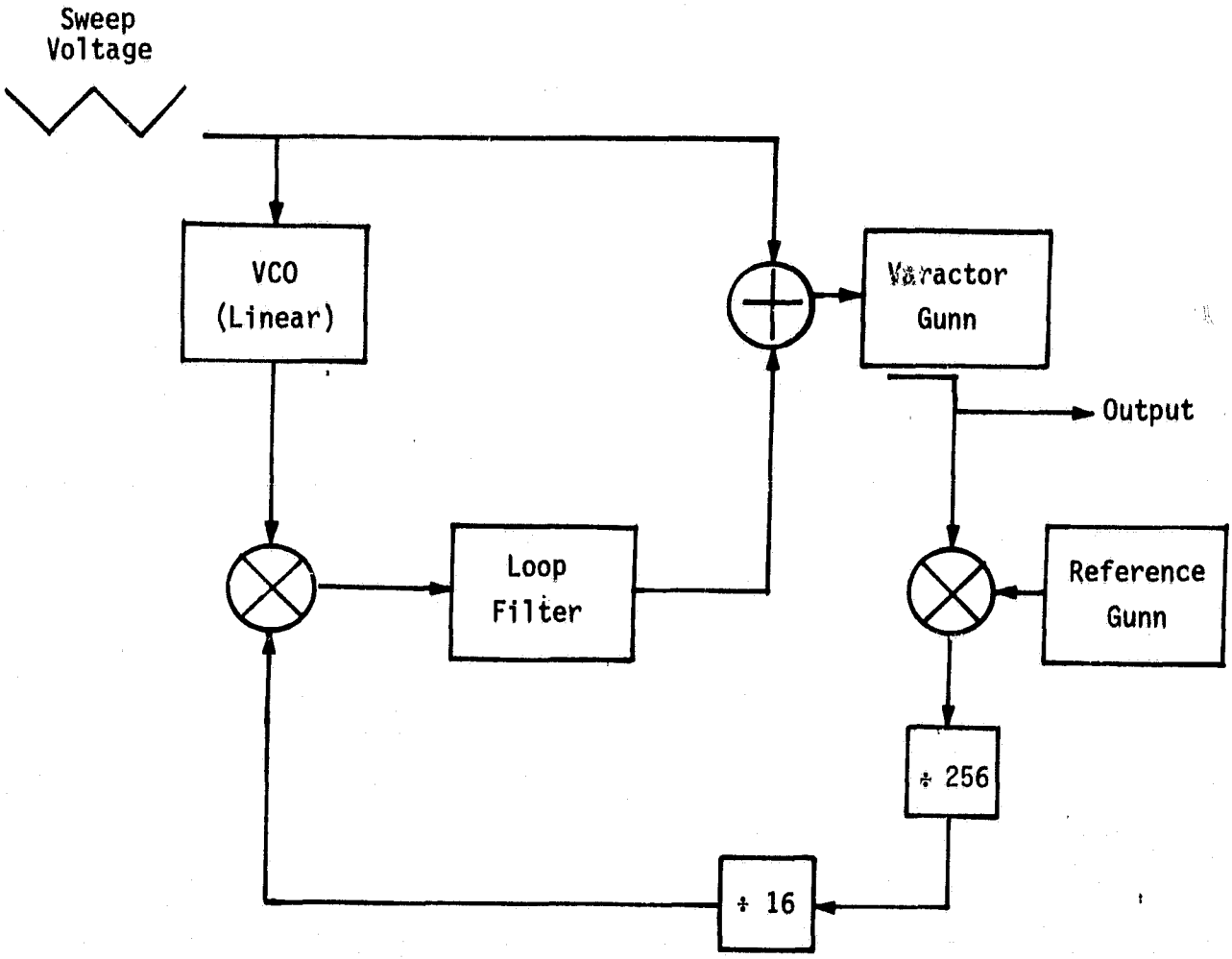


Figure 1. Radar Oscillator Model

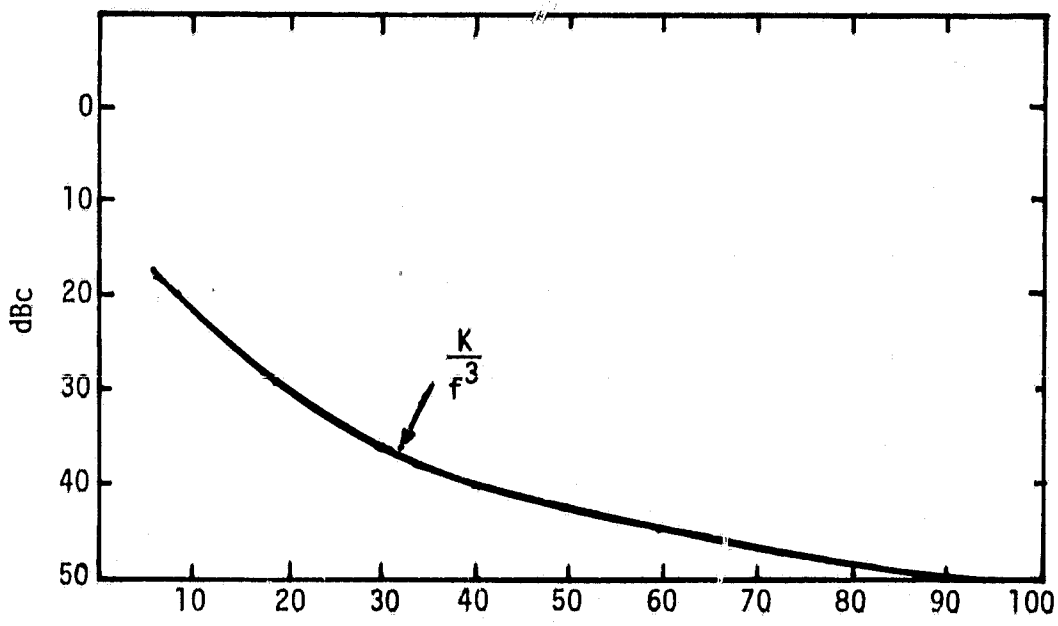


Figure 2. Phase Noise Spectral Density Model for Curve Fitting

## 3.0 OUTPUT PHASE NOISE CONTRIBUTIONS FROM EACH OSCILLATOR

In this section, we determined the transfer function of the phase noise contributions from the voltage-to-frequency converter ($VCO_1$), the Gunn oscillator and the reference oscillator. The model used for analysis is illustrated in Figure 3. In this figure, $\theta_1(t)$ is the phase noise of $VCO_1$ with zero input, $\theta_3(t)$ is the phase noise of $VCO_2$ with zero input, $\theta_4(t)$ is the phase noise due to the reference oscillator, and $\theta_2(t)$ is due to the VCO modulating voltage.

The error control signal $\varepsilon(t)$ is given by

$$\varepsilon(t) = A_1A_2A_3 \sin\left[\left(\omega_1 - \frac{(\omega_2 - \omega_3)}{M}\right)t + \theta_1 - \frac{\theta_2 + \theta_3 - \theta_4}{M}\right] \tag{2}$$

When the loop is locked, we must have (M = 4096)

$$\omega_1 = \frac{\omega_2 - \omega_3}{M} \tag{3}$$

or

$$\omega_2 = M\omega_1 + \omega_3 \tag{3}$$

so that the loop multiplies the $VCO_1$ frequency by a factor M(4096). When the system is locked, we then have

$$\varepsilon(t) = A_1A_2A_3 \sin\left(\theta_1 - \frac{\theta_2}{M} - \frac{\theta_3}{M} + \frac{\theta_4}{M}\right) \tag{4}$$

Linearizing, we have that the input to the Gunn oscillator is given by (see Figure 3)

$$\varepsilon'(t) = A_1A_2A_3\, F(s)\left[\theta_1 - \frac{\theta_2}{M} - \frac{\theta_3}{M} + \frac{\theta_4}{M}\right] \tag{5}$$

where F(s) is the loop filter transfer function expressed in the Laplace transform variable s.

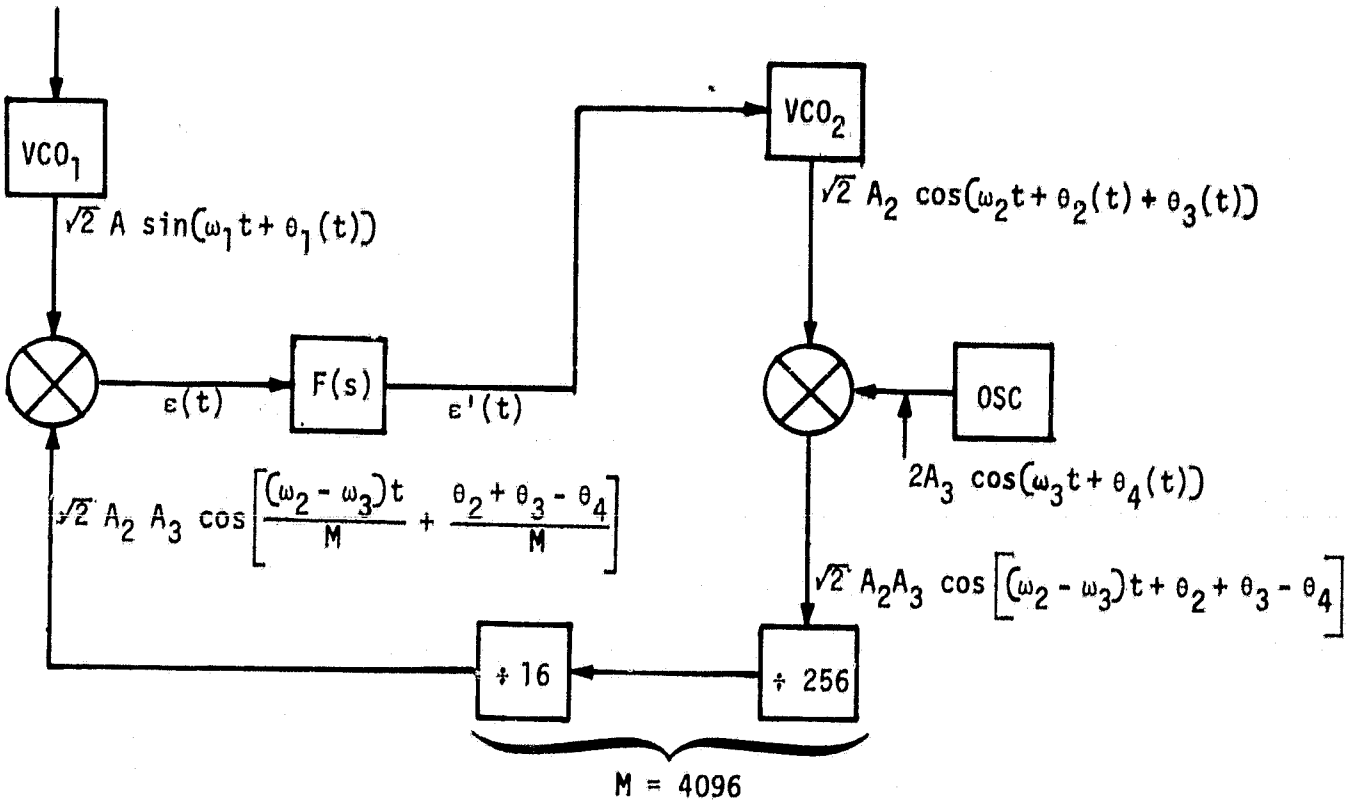


Figure 3. Model for Phase Noise Analysis

Now the phase process out of $VCO_2$ due to the input signal $e'(t)$ is given by

$$\theta_2(t) = \frac{K_2F(s)}{s}\left[\theta_1 - \frac{\theta_2}{M} - \frac{\theta_3}{M} + \frac{\theta_4}{M}\right] \tag{6}$$

or

$$\theta_2(t) = H_T(s)\left[M\theta_1(t) - \theta_3(t) + \theta_4(t)\right] \tag{7}$$

where

$$H_T(s) = \frac{K_2F(s)/(Ms)}{1 + K_2F(s)/(Ms)}$$

is the closed-loop response of the linearizing loop. It follows that the phase noise present at the output of the Gunn oscillator is given by

$$\theta_2(t) + \theta_3(t) = H_T(s)\left[M\theta_1(t) - \theta_3(t) + \theta_4(t)\right] + \theta_3(t) \tag{9}$$

or

$$\theta_2(t) + \theta_3(t) = H_T(s)\left[M\theta_1(t) + \theta_4(t)\right] + \left[1 - H_T(s)\right]\theta_3(t) \tag{10}$$

Thus, at the output of the varactor Gunn, we see that the phase of $VCO_1$ is multiplied up by the divide ratio (M=4096) and passed through a closed-loop response $H_T(s)$ which, of course, is a lowpass function. Further, the reference Gunn oscillator also has its phase noise passed through the closed-loop response $H_T(s)$. Finally, the contribution of the varactor Gunn oscillator ($VCO_2$) has its inherent (zero input) phase noise passed through $\left[1 - H_T(s)\right]$, which is a highpass function. Thus, the phase noise contribution of the voltage-to-frequency converter multiplied by 4096 (the phase noise spectral density is multiplied by $(4096)^2$) and the phase noise of the reference oscillator are the main contributors of the phase noise up to the loop natural frequency. Beyond the natural frequency, the phase noise contribution comes primarily from the varactor Gunn oscillator.

## 4.0 LOOP FILTER PARAMETERS AND LOOP BANDWIDTH

In this section, we model the loop filter in order to obtain the closed-loop bandwidth. The loop filter model shown in Figure 4 was provided by John Aker of Kustom Electronics. The transfer function is given by

$$\frac{e_0(s)}{e_i(s)} = \frac{\frac{1}{c_2 s}}{\frac{1}{c_2 s} + R_2 + \frac{R_1 \frac{1}{c_1 s}}{R_1 + \frac{1}{c_1 s}}} \tag{11}$$

After simplifying, we obtain

$$\frac{e_0(s)}{e_i(s)} = \frac{(1 + R_1 C_1 s)}{(1 + R_2 C_2 s)(R_1 C_1 s + 1) + R_1 C_2 s} \tag{12}$$

Letting

$$\begin{aligned} \tau_1 &= R_1 C_1 \\ \tau_2 &= R_2 C_2 \\ \tau_{12} &= R_1 C_2 \end{aligned} \tag{13}$$

we have

$$\frac{e_0(s)}{e_i(s)} = \frac{1 + \tau_1 s}{\tau_1 s(1 + \tau_2 s) + \tau_1 \tau_2 s^2 + \tau_{12} s} \tag{14}$$

As a first approximation, we can neglect the $s^2$ term, thus yielding

$$\frac{e_0(s)}{e_i(s)} = \frac{1 + \tau_1 s}{1 + (\tau_1 + \tau_{12} + \tau_2)s} \tag{15}$$

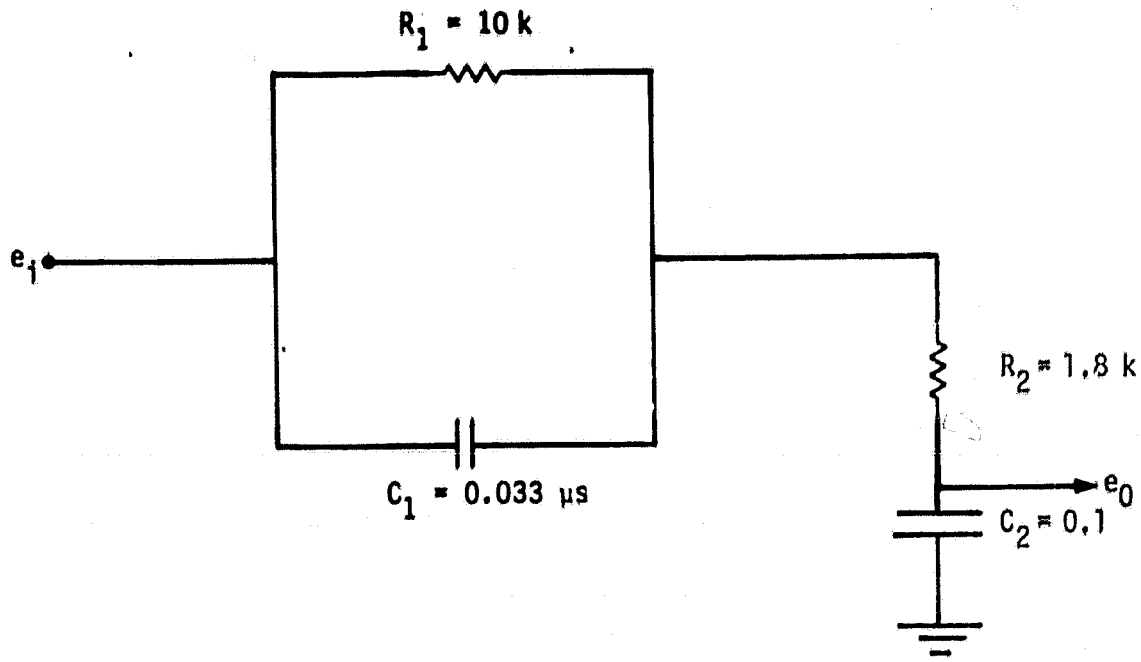


Figure 4. Loop Filter for Linearizing Loop

which is a classical passive-loop filter for a second-order phase-locked-loop (PLL). For a second-order PLL, we have

$$\omega_n^2 = \frac{AK}{(\tau_2 + \tau_{12} + \tau_1)} \tag{16}$$

and

$$\tau_1 + \frac{1}{AK} = \frac{2\zeta}{\omega_n} \tag{17}$$

where AK is the loop gain, $\zeta$ is the loop damping and $\omega_n$ is the loop natural frequency.

After evaluating, we find that

$$AK = K_\phi K_{VCO} K_{FILT} K_{DIV} \tag{18}$$

so that

$$AK = \left(\frac{4.5}{\pi}\right)(30 \times 10^6 2\pi)(0.75)\left(\frac{1}{256 \times 16}\right) = 4.94 \times 10^4 \tag{19}$$

$$\begin{aligned} \tau_1 &= 3.3 \times 10^{-4} \\ \tau_2 &= 1.8 \times 10^{-4} \\ \tau_{12} &= 0.001 \\ \omega_n &= 6.03 \times 10^3 \\ \zeta &= 1.067 \end{aligned} \tag{20}$$

and

$$B_L = \frac{\omega_n}{2}\left(\zeta + \frac{1}{4\zeta}\right) \tag{21}$$

or

$$B_L = 3{,}930 \text{ Hz} \tag{22}$$

Actually, the loop filter is followed by a three-pole Butterworth filter which has its 3-dB cutoff at 5 kHz, which serves the function of providing additional filtering beyond 5 kHz. If the three-pole Butterworth filter is modeled as an ideal lowpass filter which cuts off at 5 kHz, then it can be readily shown that the closed-loop transfer function is given by

$$H_T'(f) = H_T(f)\, F_I(f) \tag{23}$$

where $F_I(f)$ is an ideal lowpass filter with the characteristics

$$\begin{aligned} F_I(f) &= 1 && 0 < |f| < 5000 \text{ Hz} \\ F_I(f) &= 0 && |f| > 5000 \text{ Hz} \end{aligned} \tag{24}$$

This three-pole filter might be too close to the bandwidth of the closed loop since the latter is only about 20% smaller. Normally, it is not possible to model the loop as a simple second-order loop when additional filters are not at least 10 times larger in bandwidth.

## 5.0 EFFECTS OF DIFFERENCING ON PHASE NOISE

The basic range and range rate estimate is based on heterodyning the (swept) transmitted signal with the received signal. A simplified model is shown in Figure 5. From this figure, we see that the phase noise processed by the system is given by the difference

$$\Delta\theta(t) = \theta(t) - \theta(t - T) \tag{25}$$

where T is the round-trip delay time in seconds. In order to see how much low-frequency phase noise is subtracted out, we must obtain the spectral density of $\Delta\theta(t)$. Let

$$R_{\Delta\theta}(\tau) = E\Big[\big(\theta(t) - \theta(t-T)\big)\big(\theta(t+\tau) - \theta(t+\tau-T)\big)\Big] \tag{26}$$

$$R_{\Delta\theta}(\tau) = r_\theta(\tau) + R_\theta(\tau) - E[\theta(t-T)\theta(t+\tau)] - E[\theta(t)\theta(t+\tau-T)] \tag{27}$$

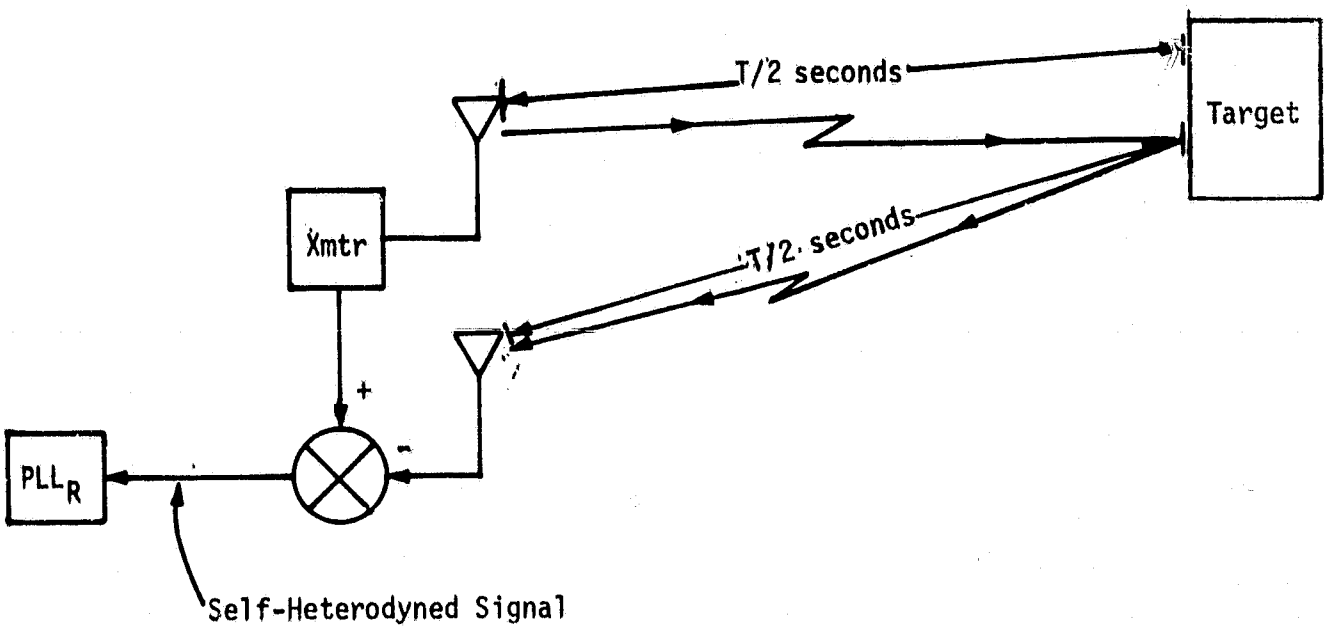


Figure 5. Model for the Self-Heterodyning

or

$$R_{\Delta\theta}(\tau) = 2R_{\theta}(\tau) - R_{\theta}(\tau+T) - R_{\theta}(\tau-T) \tag{28}$$

Taking Fourier transforms, we obtain

$$\mathcal{S}_{\Delta\theta}(f) = 2\mathcal{S}_{\theta}(f) - \int_{-\infty}^{\infty} R_{\theta}(x)\, e^{-2\pi fx}\, dx\, e^{i2\pi fT} - \int_{-\infty}^{\infty} R_{\theta}(x)\, e^{-2\pi fx}\, dx\, e^{-i2\pi fT} \tag{29}$$

After simplifying, we obtain

$$\mathcal{S}_{\Delta\theta}(f) = 2\mathcal{S}_{\theta}(f)[1 - \cos(2\pi fT)] \tag{30}$$

or, alternatively,

$$\mathcal{S}_{\Delta\theta}(f) = 4\mathcal{S}_{\theta}(f)\sin^2(\pi fT) \tag{31}$$

which is our desired result. Notice that, at low frequencies, the phase noise spectral density is weighted by a function which goes to zero as $f \to 0$. The worst-case value of T is 12 μs.

## 6.0 PHASE ERROR VARIANCE AT THE RECEIVER LOOP

In this section, we evaluate the phase error due only to the phase noise of oscillator $VCO_1$, accounting for the transmitter transfer function, the receiver transfer function and the range difference effect. It can be shown that the phase error variance is given by

$$\sigma_{\phi}^2 = 2M^2 \int_0^{5000} |H_T(f)|^2\, |1 - H_R(f)|^2\, 4\mathcal{S}_{\theta_1}(f)\sin^2(\pi fT)dt \tag{32}$$

where $H_T(f)$ is the transmitter (linearizer) closed-loop transfer function, $H_R(f)$ is the receiver PLL closed-loop transfer function, $\mathcal{S}_{\theta_1}(f)$ is the voltage-to-frequency converter phase noise spectral density and, finally, $\sin^2(\pi fT)$ is the effect of the round-trip delay on the phase noise error.

The linearizer phase noise spectral density can be modeled by

$$\begin{aligned} \mathscr{S}_{\theta_1}(f) &= 10^{-3.8}\left(\frac{40}{f}\right)^3 && 0 \leq f \leq 100 \\ \mathscr{S}_{\theta_1}(f) &= 10^{-5} && f > 100 \end{aligned} \tag{33}$$

For simplicity, we model the two transfer functions by

$$|H_T(f)|^2 = \frac{f_{n_T}^{\ 2} + 2f^2 f_{n_T}^{\ 2}}{f_{n_T}^{\ 4} + f^4} \qquad \forall f \tag{34}$$

$$|H_R(f)|^2 = \frac{f^4}{f^4 + f_{n_R}^{\ 4}} \qquad \forall f \tag{35}$$

where

$$\begin{aligned} f_{n_T} &\cong 1200 \text{ rad/s} \\ f_{n_R} &\cong 15 \text{ rad/s} \\ M &= 4096 \\ T &= 12\ \mu\text{s} \end{aligned} \tag{36}$$

Evaluating (32) produces

$$\sigma_\phi^{\ 2} \cong \overbrace{8(4096)^2\,\pi^2\,T^2 \int_0^{100} \frac{f^6}{f^4 + f_{n_R}^{\ 4}}\, 10^{-3.8}\,\frac{(40)^3}{f^3}\,df}^{I_1}$$

$$+ \overbrace{8(4096)^2\,\pi^2\,T^2 \int_{100}^{5000} \frac{\left(f_{n_T}^{\ 4} + 2f^2 f_{n_T}^{\ 2}\right) f^2}{f_{n_T}^{\ 4} + f^4}\, 10^{-5}\,df}^{I_2} \tag{37}$$

Evaluate $I_1$:

$$I_1 = 8(4096)^2 \pi^2 \left(12\text{x}10^{-6}\right)^2 10^{-3.8} (40)^3 \int_0^{100} \frac{f^3}{f^4 + f_{n_R}^4} df \quad (38)$$

or

$$I_1 = 3.57 \text{ rad}^2 \quad (39)$$

Now consider $I_2$:

$$I_2 = 8(4096)^2 \pi^2 T^2 \int_0^{5000} \frac{\left(f_{n_T}^4 + 2f^2 f_{n_T}^2\right) f^2}{f_{n_T}^4 + f^4} 10^{-5} df$$

$$\cong 8(4096)^2 \pi^2 T^2 \left[ \int_{100}^{1200} 10^{-5} \sqrt{\tfrac{3}{2}} f^2 df + \int_{1200}^{5000} 10^{-5}(2)(1200)^2 df \right] \quad (40)$$

and

$$I_2 = 2.49\text{x}10^4 \text{ rad}^2 \quad (41)$$

Hence,

$$\sigma_\phi^2 \cong 2491 \text{ x } 10^4 \text{ rad}^2 \quad (42)$$

or

$$\sigma_\phi \cong 158 \text{ rad} \quad (43)$$

Based on classical PLL theory, this value of phase suggests that a tracking problem could exist; however, it is not clear that a phase error at frequency components well above the natural frequency of the loop are important. In fact, it is rather difficult to understand how this can be important in losing lock since the loop cannot respond to frequencies well above the loop natural frequency.

In conclusion, it is believed that the voltage-to-frequency converter $VCO_1$ should be selected with a lower phase noise spectral density which, in fact, has already been done.

# APPENDIX B

## CIRCUIT DRAWINGS

# APPENDIX C

# SOFTWARE LISTING

# APPENDIX D

## LIST OF NONSTANDARD COMPONENTS

KUSTOM ELECTRONICS
8320 Nieman Road, Lenexa, Kansas 66214 • (913) 492-1400
Telex WUD (0) 37437 • Cable Address: KUSTOMELEC



May 10, 1982

Mr. Peter Nilsen
Axiomatix
9841 Airport Boulevard
Suite 912
Los Angeles, CA 90045

Dear Peter:

I have listed below the part numbers for the non-standard components used in the NASA Space Radar:

a. Mixer Diode Assembly
   Kustom Part Number 200-0544-00, modified with a special 10-inch cable similar to 155-2045-00.
b. CPU Chip
   Motorola MC68701L, with Kustom "RADARS3 012582" program.
c. Low Power Gunn Oscillator
   Kustom Part Number 015-0045-00.
d. Varactor-tuned Gunn Oscillator
   Varian Model No. VSK9014AT
   Order From: Varian Solid State Microwave Division
   3251 Olcott Street
   Santa Clara, CA 95050

The first three parts can be obtained directly from Kustom; please use me as your contact in the event you wish to order any of these.

I am looking forward to hearing from you on the results of the NASA tests.

Sincerely,

John Kusek

John Kusek
Senior Engineering Manager

JK/dd

# APPENDIX E

## PREACCEPTANCE TEST DATA

KUSTOM ELECTRONICS
8320 Nieman Road, Lenexa, Kansas 66214 • (913) 492-1400
Telex WUD (0) 437437 • Cable Address: KUSTOMELEC

April 20, 1982

Mr. Peter Nilsen
Axiomatix
9841 Airport Boulevard
Suite 912
Los Angeles, CA 90045

Dear Peter:

The following sheets are the results of the tests we have performed with the Axiomatix Radar during the last week. Data was obtained using two different targets and using two different approaches to verifying velocity depending upon the range and velocities involved. Data taken from the range of 100 meters and less was obtained using the corner reflector as the target. The corner reflector was situated where we would get a minimum amount of interference from background objects. At distances greater than 400 meters we used the water tower as the target.

Range rate measurements of approximately 3/10 of a meter per second and above were obtained by aiming the radar at the target from a moving vehicle. Vehicle speed was verified by the use of a Kustom HR-4 Police Radar which had been modified to readout in 10ths of meters per second. As the vehicle passed through the indicated range, readings were simultaneously taken from the Axiomatix Radar and from the HR-4 Unit. This procedure was conducted in both the approaching and receding modes.

Lower speed measurements were conducted by mounting the radar in a toy wagon. The wagon was pulled by a variable speed winch over a wooden track about 3 meters long. Once the speed of the wagon had stablized the elapsed time taken by the wagon to travel over a measured 1 meter distance was measured with a stopwatch. From this we calculated the speed of the wagon in meters per second. This was used as the standard of comparison for the Axiomatix Radar Unit Readings. This test was also, conducted in both the approaching and receding modes.

Please give me a call if you have any questions after you have had a chance to review these findings. We are looking forward to seeing you on the 4th. In the meantime, we still plan on sending up the weather balloon and getting some longer range measurements if the weather will cooperate. I will keep you advised on this.

Sincerely,

John Kusek

John Kusek
Senior Engineering Manager

JK/dd

Enclosures

# NASA RADAR TEST

## Radar Test

Following data taken using long range search $\sum \frac{X^2}{N} = .02$ M/Sec

Readings taken over
1 Meter

| DISTANCE | SEC (FOR 1 METER) | CALCULATED SPEED M/SEC | AVERAGE READING | STATIC READING M/SEC | CORRECTED READING M/SEC |
|---|---|---|---|---|---|
| 438 M | 5.7 | + .175 | + .15 | - .02 | + .17 |
| 438 M | 4.6 | - .217 | - .27 | - .02 | - .25 |
| 438 M | 6.3 | + .159 | + .14 | - .02 | + .16 |
| 38 M | 11.0 | - .091 | - .11 | - .02 | - .09 |
| 438 M | 8.4 | - .119 | - .17 | - .02 | - .15 |
| 438 M | 11.2 | + .089 | + .08 | - .02 | + .10 |
| 438 M | 7.4 | + .135 | + .12 | - .02 | + .14 |
| 438 M | 4.1 | - .244 | - .29 | - .02 | - .27 |

Approaching (-) Receeding (+)

NASA RADAR TEST

LONG RANGE RATE TEST

| DISTANCE (METERS) | AXIOMATIX M/SEC | HR-4 M/SEC | A = APPROACHING (-) R = RECEEDING (+) |
|---|---|---|---|
| 1. 500 | - 1.17 | 1.1 | A |
| 2. 500 | + 1.00 | 1.0 | R |
| 3. 500 | - 1.67 | 1.6 | A |
| 4. 500 | + 1.67 | 1.6 | R |
| 5. 500 | - 4.30 | 4.4 | A |
| 6. 500 | + 4.59 | 4.5 | R |
| 7. 500 | - 7.00 | 6.7 | A |
| 8. 500 | + 0.63 | 0.6 | R |
| 9. 500 | - 0.50 | 0.4 | A |
| 10. 500 | + 0.35 | 0.3 | R |

# NASA RADAR TEST

## Range Rate

| DISTANCE | SEC (FOR 1 METER) | CALCULATED SPEED M/SEC | AVERAGE READING | STATIC READING M/SEC | CORRECTED READING M/SEC |
|---|---|---|---|---|---|
| 100 M | 8.6 | + .116 | + .09 | - .03 | + .12 |
| 100 M | 5.9 | - .169 | - .24 | - .05 | - .19 |
| 100 M | 5.5 | - .182 | - .29 | - .05 | - .24 |
| 100 M | 9.6 | + .104 | + .04 | - .05 | + .09 |
| 100 M | 6.9 | + .144 | + .12 | - .03 | + .15 |
| JO M | 5.4 | + .185 | + .17 | - .02 | + .19 |
| 50 M | 4.2 | + .238 | + .31 | + .03 | + .28 |
| 50 M | 3.9 | + .256 | + .32 | + .04 | + .28 |
| 50 M | 7.8 | - .128 | - .12 | + .01 | - .13 |
| 50 M | 16.5 | - .060 | - .18 | - .01 | - .07 |
| 50 M | 11.8 | + .085 | + .09 | - .01 | + .10 |
| | Readings Taken Over 4.66 Meters | | | | |
| 5M | 44.7 | - .104 | -.09 | + .01 | - .10 |
| 5M | 38.1 | + .122 | + .13 | + .02 | + .11 |

Approaching (-) Receeding (+)

Date 4-20-82

NASA Radar Test

Aquisition Time

| TEST | Short Range 10 Meters | Medium Range 140 Meters |
|---|---|---|
| 1 | 1.2 sec | 5.5 sec |
| 2 | 1.5 sec | 6.0 sec |
| 3 | 1.5 sec | 6.0 sec |
| 4 | 1.5 sec | 5.5 sec |
| 5 | 1.5 sec | 6.0 sec |

# APPENDIX F

# BREADBOARD LAYOUT

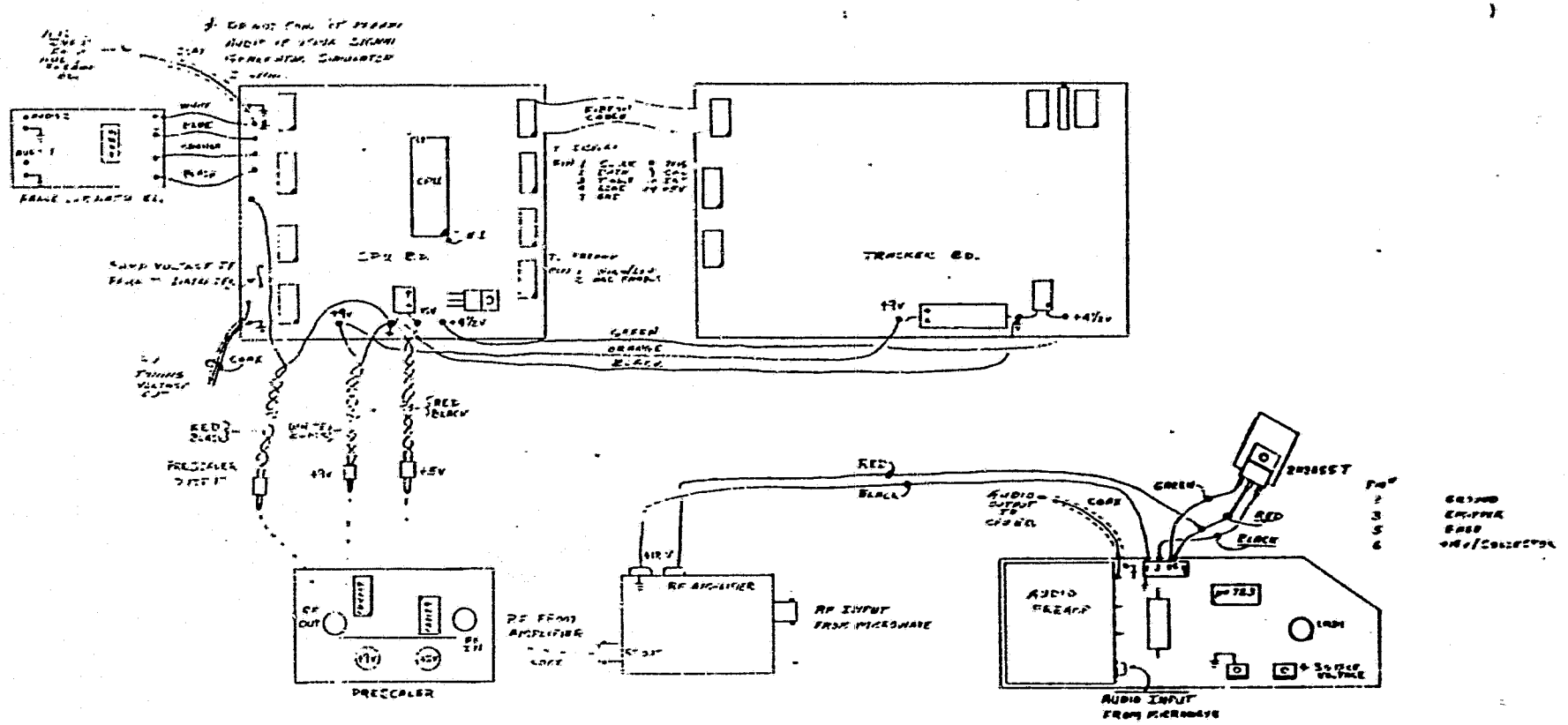


NASA/AXIOMATIX RADAR

KUSTOM ELECTRONICS
MAY 1982
S Hicker

# APPENDIX G

## CDR BREADBOARD TEST RESULTS

Axiomatix

9841 Airport Boulevard • Suite 912 • Los Angeles, California 90045 • Phone (213) 641-8600

TECHNICAL MEMORANDUM NO. M8103-1

| | | | |
|---|---|---|---|
| To: | Bill Goodson, Kustom Electronics | Date: | March 4, 1981 |
| From: | Peter Nilsen<br>Sergei Udalov | Copies: | G. Huth<br>A. Pajak, NASA |
| Subject: | CDR Radar Test Results | Contract: | NAS 9-15666 |

---

The test data for the range measurement experiment which we performed at the CDR is given in Table 1. This data represents raw, unsmoothed data. In order to get some appreciation of how simple processing, such as a simple averager, might improve the accuracy, the following "processing" was applied to the raw data. The 50 measurements were grouped into five groups of 10 measurements. Each group of 10 was averaged

$$\overline{R_j} = \frac{\sum_{i=1}^{10} R_i}{10}, \qquad j=1 \text{ to } 5$$

such that $\overline{R_j}$ represents an averaged range measurement that the radar could easily calculate. The standard deviation of the five $\overline{R_j}$ was calculated to be 6 cm, or 0.04% of the measured range. The standard deviation of 20 nonaveraged measurement values was calculated and found to be 19 cm. Thus, it appears that the simple technique of averaging a relatively small number of measurements and displaying the averaged value can provide accuracy improvement by a factor of three. At this point, it should be stressed that we are not claiming that this averaging is optimum or that the factor of three improvement is always guaranteed to be achievable. However, we do think that relatively simple techniques can be used to improve the radar performance. It should also be stressed that such an averaging technique in no way reduces errors due to biases in the system (if they exist).

Table 1. CDR Test Data

| Raw Measurements (meters) | Mean and σ of Group of 10 | Raw Measurements (meters) | Mean and σ of Group of 10 |
|---|---|---|---|
| 1. 137.2 | | 31. 136.8 | |
| 2. 137.2 | | 32. 137.2 | |
| 3. 137.2 | | 33. 136.9 | |
| 4. 136.9 | $\bar{R}_1$ = 136.91 | 34. 137.0 | $\bar{R}_4$ = 136.92 |
| 5. 136.9 | | 35. 136.9 | |
| 6. 136.8 | $\sigma_1$ = 0.22 | 36. 136.8 | $\sigma_4$ = 0.15 |
| 7. 136.8 | | 37. 137.0 | |
| 8. 136.6 | | 38. 136.8 | |
| 9. 136.7 | | 39. 136.8 | |
| 10. 136.8 | | 40. 136.8 | |
| 11. 136.9 | | 41. 136.9 | |
| 12. 137.1 | | 42. 136.8 | |
| 13. 137.1 | | 43. 137.0 | |
| 14. 137.1 | $\bar{R}_2$ = 136.96 | 44. 137.0 | $\bar{R}_5$ = 136.87 |
| 15. 137.1 | | 45. 136.8 | |
| 16. 136.8 | $\sigma_2$ = 0.15 | 46. 137.0 | $\sigma$ = 0.19 |
| 17. 136.8 | | 47. 137.1 | |
| 18. 136.7 | | 48. 136.8 | |
| 19. 137.0 | | 49. 136.8 | |
| 20. 137.0 | | 50. 136.9 | |
| 21. 136.7 | | | |
| 22. 136.7 | | | |
| 23. 136.7 | | | |
| 24. 136.7 | $\bar{R}_3$ = 136.81 | | |
| 25. 136.8 | | | |
| 26. 136.8 | $\sigma_3$ = 0.13 | | |
| 27. 136.9 | | | |
| 28. 136.6 | | | |
| 29. 137.0 | | | |
| 30. 137.0 | | | |

A few comments about the experiment are in order, as follows:

1. The test environment, i.e., the parking lot, was far from ideal. There was undoubtedly a large amount of multipath and clutter.

2. Considering this environment and that the radar had been "lashed together" only a few hours earlier, it is impressive that a standard deviation of 0.04% was achieved.

Peter Nilsen

Peter W. Nilsen

/lp